Published in final edited form as:

Neuron. 2021 October 06; 109(19): 3104–3118.e6. doi:10.1016/j.neuron.2021.07.018.

Oligodendroglial Ring Finger Protein Rnf43 is an essential injury specific regulator of oligodendrocyte maturation

Jianqin Niu[1,2,3,4,*], **Guangdan Yu**[3], **Xiaorui Wang**[3], **Wenlong Xia**[1], **Yuxin Wang**[3], **Kimberly K. Hoi**[1], **Feng Mei**[3,4], **Lan Xiao**[3,4], **Jonah R. Chan**[1,5], **Stephen P.J. Fancy**[1,2,5,6,7,*]

[1.]Department of Neurology, University of California at San Francisco, San Francisco, CA 94158, USA

[2.]Department of Pediatrics, University of California at San Francisco, San Francisco, CA 94158, USA

[3.]Department of Histology and Embryology, Third Military Medical University, Chongqing 400038, China

[4.]Institute of brain and intelligence, Third Military Medical University, Chongqing 400038, China

[5.]Division of Neuroimmunology and Glial Biology, University of California at San Francisco, San Francisco, CA 94158, USA

[6.]Newborn Brain Research Institute, University of California at San Francisco, San Francisco, CA 94158, USA

[7.]Lead Contact

Summary

Oligodendrocyte (OL) maturation arrest in human white matter injury significantly contributes to the failure of endogenous remyelination in multiple sclerosis (MS) and newborn brain injuries such as Hypoxic Ischemic Encephalopathy (HIE) that cause cerebral palsy. Here we identify an oligodendroglial intrinsic factor that controls OL maturation specifically in the setting of injury. We find a requirement for the Ring Finger Protein Rnf43 not in normal development, but in neonatal hypoxic injury and remyelination in the adult mammalian CNS. Rnf43, but not the related Znrf3, is potently activated by Wnt signaling in oligodendrocyte progenitor cells (OPCs) and marks activated OPCs in human MS and HIE. Rnf43 is required in an injury-specific context, and promotes OPC differentiation through negative regulation of Wnt signal strength in OPCs

[*]Correspondence: jianqinniu@163.com (J.N.), stephen.fancy@ucsf.edu (S.P.J.F.).

Author Contributions

J.N. and S.P.J.F. conceived the study. J.N. and S.P.J.F. designed the experiments and analyzed the data. J. N., G.Y., X. W., W.X., Y.W., K.K.H. and S.P.J.F. performed experiments. F.M., L.X., J.R.C provided reagents and intellectual contributions. J. N. and S.P.J.F wrote the paper.

Declaration of Interests

The authors declare no competing interests.

at the level of Fzd1 receptor presentation on the cell surface. Inhibition of Fzd1 using UM206 promotes remyelination following ex vivo and in vivo demyelinating injury.

Graphical Abstract

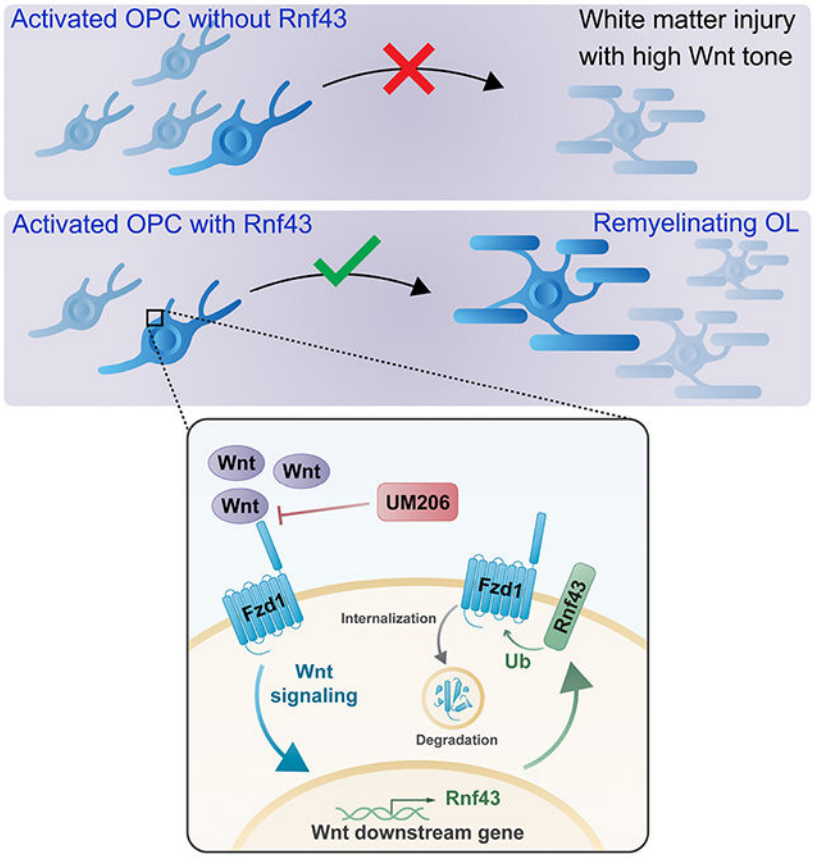

In Brief

Niu et al. identify a factor, Rnf43, that marks activated oligodendrocyte progenitors (OPCs) in human white matter injury, that is required in an injury specific context for their maturation and successful remyelination, and acts by regulating Wnt signal strength at the level of OPC surface presentation of Wnt receptor Fzd1.

Introduction

Permanent damage to white matter tracts, comprising axons and myelinating oligodendrocytes, is an important component of multiple sclerosis (MS) as well as newborn brain injuries that cause cerebral palsy (CP). In MS, the most common cause of neurological disability in young adults, myelin sheaths are lost through injury or death of mature oligodendrocytes (OL) as a result of autoimmune damage [Reich et al., 2018]. White matter disorders are also associated with human newborn neurological injuries leading to CP [Volpe, 2009; Silbereis et al., 2010]. In these conditions, myelin sheaths can be regenerated by oligodendrocyte progenitor cells (OPCs) that are recruited to lesions and differentiate in

a process called remyelination [Franklin and Ffrench-Constant, 2017]. Evidence suggests that myelin repair often fails in MS and CP, and that OPCs are unable to differentiate into mature myelin-forming OL [Chang et al., 2002; Wolswijk et al., 1998; Billiards et al., 2008]. This inhibition of OPC differentiation, remyelination failure, and axonal loss of myelin trophic support, contributes significantly to ongoing neurological dysfunction, axonal loss and disease progression. It is therefore critical to understand mechanisms underlying the failure of endogenous remyelination in human injury.

Much has been learnt about the regulation of oligodendrocyte biology in remyelination from the study of development, and indeed the recapitulation hypothesis of myelin regeneration proposes that the oligodendroglial intrinsic program underlying remyelination after injury is essentially a rerunning of a developmental myelination program [Fancy et al., 2011a]. However, human myelin repair is susceptible to failure, despite the robustness of developmental myelination, suggesting key differences in the regulation and propensity for dysregulation of the two processes. Several cellular signaling pathways involved in the OL program of developmental myelination have been implicated in the remyelination program [Gallo and Deneen, 2014]. However, less is understood about whether there are oligodendroglial intrinsic factors that operate specifically in the setting of injury but not in normal development, and how these might become dysregulated.

Ring Finger Protein 43 (Rnf43) was first identified in intestinal crypt stem cells, along with the related RING-type E3 ubiquitin ligase Znrf3 (Zinc and Ring Finger 3) [Koo et al., 2012, Hao et al., 2012], and both contain an extracellular ectodomain, a single transmembrane region and a cytoplasmic RING domain. They are targets of Wnt signaling as well as functioning as negative feedback repressors of the pathway. They regulate Wnt signal strength by ubiquitinating Frizzleds, the cell membrane receptors for Wnt ligands, and targeting them to the lysosomal degradation pathway [Koo et al., 2012, Hao et al., 2012; Planas-Paz et al., 2016; Szenker-Ravi et al., 2018]. In the intestinal crypt compartment and other organ systems, Rnf43 and Znrf3 are co-expressed and are able to compensate for each other’s loss, and only with simultaneous loss of both ligases do cells become hypersensitive to locally secreted Wnt [Koo et al., 2012]. In the oligodendrocyte lineage, Wnt signaling is a potent inhibitor of OPC maturation [Fancy et al., 2009; Ye et al., 2009, Feigenson et al., 2009; Fancy et al., 2011b; Lee et al., 2015], acting as a checkpoint controlling the timing of OL differentiation, and preventing further maturation during both developmental myelination and remyelination. Evidence suggests that the pathway can become dysregulated in human white matter injury (WMI), and that a pathologically high Wnt signaling tone can exist in OPCs that may account for their maturation arrest [Fancy et al., 2014].

This Wnt tone in cells is regulated by a fine balance between pathway activators and repressors [Clevers, 2006]. Here we demonstrate an injury specific pathway repressor in OPCs that functions to control OL maturation kinetics specifically in the context of myelin regeneration. We find that Rnf43 is potently activated by Wnt signaling in OPCs, serving as a marker of activated OPCs in human WMI. Loss of Rnf43 during development does not affect the timely developmental program of myelination, but during injury repair causes significant remyelination delay with permanent deficits.

Results

Rnf43 identifies activated OPCs in human white matter injury and is a target of Wnt

Analysis of both human and mouse identifies expression of Rnf43 in a cell and injury specific pattern in the adult CNS. RNF43 protein expression is detected in cells with the simple bipolar morphology of OPCs in human WMI in both MS (Fig. 1A, B) and neonatal HIE (Fig. 1C, D). RNF43 expression colocalizes with the OPC marker PDGFRα in human white matter injury, and not with markers for other cell types such as astrocytes and microglia. (Fig. 1E, quantification in Fig. S1G). RNF43 is expressed in OPCs within active MS lesions (Fig. 1B 'Active', 1G), but is absent in OPCs in surrounding normal appearing white matter in these same patients (Fig. 1B 'NAWM', 1G). Similarly we find RNF43 activation in OPCs in human neonatal HIE (Fig. 1C, D, Fig. S1A), but absence in white matter of age matched human control cases (Fig. S1A, quantification in Fig. S1B). RNF43 is expressed extensively in OPCs throughout the white matter in HIE (Fig. 1D 'WM', 1E, 1F, 1G) but shows a striking lack of expression in grey matter OPCs in these patients (Fig. 1D 'GM', 1F, 1G), which can be seen most clearly at the boundary of grey and white matter regions (Fig. 1F). An injury specific expression of Rnf43 in human injury is supported by evidence from murine adult CNS tissue. Rnf43 is not expressed in the adult uninjured mouse CNS (Fig. 1I 'No Lesion') of PDGFRα-YFP reporter mice (in which OPCs are labelled with YFP), but is activated and expressed by OPCs in murine remyelination (Fig. 1I 'lesion', 1H, Fig. S1D, E). We also find a marked upregulation of Rnf43 in OPCs in neonatal white matter injury, at P10 in PDGFRα-YFP reporter mice exposed to chronic hypoxia compared to normoxic controls (Fig. S1C, D, F).

Rnf43 has been identified as a Wnt pathway target in various biological systems [Koo et al., 2012, Hao et al., 2012]. We find that Rnf43 is also regulated by Wnt signaling in OL lineage, and is significantly activated by the pathway. Wildtype OPCs exposed to increasing levels of the Wnt ligand Wnt3a in vitro (Fig. 2A), and OPCs isolated from Olig2cre:APCfl/fl mice (Fig. 2B)(which have excessive Wnt activation due to the conditional loss of the obligate pathway repressor adenomatous polyposis coli (APC)) demonstrate significant increases in the expression of Rnf43 mRNA (Fig.2A), along with other established Wnt targets such as Axin2 and Notum (Fig. 2A, B). In other Wnt responsive tissues, Rnf43 is activated along with the related Ring Finger Protein Znrf3, and the two are able to functionally compensate for each other. In contrast however, we find that Znrf3 is not detectable, nor is a target of Wnt signaling, in OL lineage. Znrf3 mRNA is not upregulated by Wnt3a in OPCs (Fig. 2A), or in OPCs isolated from Olig2cre:APCfl/fl (Fig. 2B), suggesting a tissue specific difference in regulation in OL lineage. Similar results are found in the expression of Rnf43 and Znrf3 proteins. Rnf43 protein is significantly upregulated in OPCs isolated from Olig2cre:APCfl/fl mice compared to control (Fig. 2C, D), whilst Znrf3 protein is not detectable in either wildtype or Olig2cre:APCfl/fl OPCs (Fig. 2D). Consistent with Rnf43 being a target of Wnt, we find it that it is expressed in a maturational stage specific manner in OL lineage (Fig. 2E, F). Rnf43 protein and mRNA expression marks Wnt activation in OPCs, but both are downregulated coincident with the downregulation of Wnt pathway that is required for OL maturation into MBP-expressing cells, (Fig. 2E, F). Rnf43 is also regulated by Wnt signaling during remyelination in vivo. Rnf43 protein is significantly

upregulated specifically in Olig2+ cells at 5 days post lesioning (5dpl) following stereotaxic lysolecithin injection into corpus callosum of PDGFRα-creER:APCfl/fl mice (Fig. 2G, 2H) (which have excessive Wnt activation in OPCs due to induceable loss of APC), and total intralesional Rnf43 mRNA is also significantly increased in these mice, whereas Znrf3 is unaltered (Fig. 2I). Together these results suggest that Rnf43 is regulated by Wnt signaling in OPCs, and is expressed in OPCs in an injury specific pattern in the adult CNS in both mouse and human.

Rnf43 functions in an injury specific context and is essential for remyelination

Rnf43 and Znrf3 can functionally compensate for each other in various biological systems [Koo et al., 2012, Hao et al., 2012]. We therefore assessed both factors in development of OL lineage, despite lack of evidence for Znrf3 expression or regulation by Wnt in OL. We crossed either Olig1-cre or Olig2-cre mice (for conditional ablation in OL lineage) with Rnf43 and Znrf3 floxed lines (double Rnf43/Znrf3 floxed referred to hereafter as RZfl/fl) to generate both Olig1cre:RZfl/fl and Olig2cre:RZfl/fl double conditional knockout mice. Despite a transient expression of Rnf43 in OPCs during development (Fig. S2A–E), both Rnf43 and Znrf3 functions are dispensable for timely developmental myelination. Double Olig1cre:RZfl/fl conditional knockouts show normal amounts of MBP protein in multiple brain regions at P10 and P14 (Fig. 3A), including corpus callosum (Fig. 3B). Similar results were found for MBP protein in Olig2cre:RZfl/fl mouse brain at P10 (Fig. S2F–G). There is no difference in *PLP-DM20+* cell number at P5 in Olig1cre:RZfl/fl mice corpus callosum (Fig. S3A–B). There is a transient reduction in MAG+ cell number at P7 and MBP expression at P10 in corpus callosum of Olig1cre:RZfl/fl mice but these have normalized by P10 and P14 respectively (Fig. S3A–B, Fig. 3B). No differences are seen in *MAG*+ cell number in spinal cord at either P7 or P10 (Fig. S3C–D). Normal numbers of *MAG* mRNA expressing oligodendrocytes are seen in developing corpus callosum by both P10 and P14 (Fig. 3C, D), associated with normal numbers of myelinated axons (Fig. 3F, p=0.96) and morphological thickness of myelin at P21 (Fig. 3E, G).

Functional analysis in adult remyelination however identifies critical function for normal repair kinetics. We crossed an inducible PDGFRα-CreER line to Rnf43 and/or Znrf3 floxed lines and generated single and double conditional mutants of Rnf43 and Znrf3. Following lysolecithin induced demyelination in the corpus callosum of adult double conditional knockout mice (PDGFRα-CreER:RZfl/fl)(Fig. S4A lesioning schematic) or control mice (Cre negative, RZ fl/fl mice), we find a significant reduction in MAG expressing mature OL in lesions of double mutants at 10dpl (P=6.75E-4, 2.2 fold reduction) that persists at 21dpl (p=2.77E-7, 2.4 fold reduction)(Fig. 4A–B), in the presence of normal numbers of total Olig2+ cells at both times (Fig. 4C–D) and unchanged proportions of Olig2+ cells that are proliferating (Fig. S5A–B). Remyelination is severely hampered in double mutants, with significant reductions in MBP protein in lesions at both 10dpl and 21dpl (P=1.67E-4, 10 fold reduction at 10dpl, p=0.00145, 3.2 fold reduction at 21dpl)(Fig. 4E–F), and significant reductions at 14dpl and 21dpl in both the number of remyelinated axons in lesions (p=0.00147, 4 fold reduction at 14pdl, p=0.0021, 2.1 fold reduction at 21dpl)(Fig. 4G–H) and the thickness of myelin in those axons that are remyelinated (Fig. 4G, J). Consistent with our finding that Znrf3 is not expressed in OPCs nor is a target of Wnt signaling in

OL lineage, this repair deficit in the Rnf43/Znrf3 double mutant is attributable to Rnf43 function rather than Znrf3. Analysis of single PDGFRα-creER:Rnf43fl/fl and PDGFRα-creER:Znrf3fl/fl mutants shows that single Rnf43 loss of function mice show a similar reduction in MAG expressing mature OL at 14dpl as Rnf43/Znrf3 double mutants (Fig. 4K–L), whereas single Znrf3 mutants are not significantly different from wildtype littermate controls (Fig. 4K–L). Loss of Rnf43 function leads to persistent defects in remyelination, and analysis at 50dpl extended lesion time points suggests permanent reductions in myelin thickness (Fig. 4I–J, Fig. S5F, H), despite normalization of CC1-expressing mature OL numbers and normalization of MBP protein intensity (Fig. S5). We also find that Rnf43 has critical injury specific function in the setting of neonatal white matter injury. Chronic neonatal hypoxia from P3 to P10 in RZfl/fl control mice (non Cre mice) leads to deficits in numbers of *MAG*+ OL and MBP protein expression in the corpus callosum compared to normoxic animals, but loss of Rnf43 in OPCs in Olig1cre:RZfl/fl mice markedly and significantly exacerbates this OL maturation block during hypoxia (Fig. S6A–F). As in adult remyelination, use of single Olig1-cre:Rnf43fl/fl and Olig1-cre:Znrf3fl/fl mutants in neonatal hypoxia shows that Rnf43 is required, but Znrf3 does not participate (Fig. S6G–H). Together these results identify critical injury specific functions for Rnf43, but not Znrf3, in the control of OL maturation kinetics, that are not required for the timely developmental OL program of myelination.

Rnf43 controls OPC differentiation through negative regulation of Wnt

Activation of the Wnt pathway in OPCs potently blocks their maturation into mature OL, and Wnt tone must be extinguished for OPC differentiation [Fancy et al., 2009; Ye et al., 2009, Feigenson et al., 2009; Fancy et al., 2011b; Lee et al., 2015]. Whilst the Rnf43 gene serves as a target of pathway activation, we find that the protein functions as a critical negative feedback mechanism to control pathway activation. We find that Rnf43 controls OL differentiation through repression of Wnt pathway, and that loss of Rnf43 makes OPCs hypersensitive to extracellular Wnt ligand. OPCs isolated from Olig1cre:RZfl/fl mice show significantly reduced differentiation in vitro compared to those isolated from control littermate mice even in the absence of Wnt3a ligand added into the medium (Fig. 5A, B. Fig. 5B 0ng/ml: Olig1cre:RZ fl/fl vs. RZ fl/fl p=0.00689, 2.9 fold reduction at 2 days. p=0.014, 1.6 fold reduction at 4 days). This effect even in the absence of added Wnt ligand is likely because cultured OPCs inherently demonstrate an elevated Wnt tone due to their own production and secretion of Wnt ligands that act in an autocrine manner as previously published [Yuen et al., 2014](treatment of OPC cultures and myelinating co-cultures with porcupine inhibitor IWP2 has been shown to promote their differentiation and myelination, by inhibiting their release of Wnt ligands [Yuen et al., 2014]). Use of individual Olig1cre:Rnf43fl/fl and Olig1cre:Znrf3fl/fl single conditional mutants demonstrates that these effects on differentiation are attributable to loss of Rnf43 function rather than Znrf3 (Fig. S7A–B). Increasing exposure of wildtype OPCs to Wnt3a ligand leads to reductions in differentiation into MBP+ protein expressing cells both at 2 days and 4 days post differentiation, and this effect is significantly exacerbated in Olig1cre:RZfl/fl OPCs (p=0.00813, 6.3 fold differentiation reduction at 2d with 2ng/ml; p=8.59E-4, 16.7 fold differentiation reduction at 4d with 2ng/ml)(Fig. 5A, B). Considering the functional role of Rnf43 in adult remyelination, it would be an interesting consideration whether OPCs

isolated from aged adult Rnf43 knockout mice would be more hypersensitive to Wnt ligand than their neonatal counterparts. This hypersensitivity to extracellular Wnt ligand in the absence of Rnf43 is also reflected in elevated Wnt pathway activation in OPCs in response to Wnt3a stimulation (Fig. 5C), as evidenced by significantly elevated mRNA levels of pathway targets such as *Axin2* (p=0.044, 2.23 fold increase) and *Notum* (p=7.87E-4, 6.61 fold increase). Conversely, gain of Rnf43 function silences Wnt pathway activation and promotes differentiation and initiation of MBP expression (Fig. 5D–F). Transfection of the Oli-neu cell line with vector expressing Rnf43 (Fig. 5D) leads to reduced Wnt pathway activation in response to increasing Wnt3a exposure (Fig. 5E)(evidenced by reduced Wnt target Axin2 mRNA levels), and prevents the differentiation blocking effects of this Wnt ligand administration (Fig. 5F). Rnf43 also acts to repress Wnt pathway in vivo in OPCs during remyelination. Similar upregulation of the Wnt target *Axin2* is seen in OPCs in 7dpl remyelinating lesions from both PDGFRα-creERT:APCfl/fl mice (Fig. 5G)(in which OPCs have lost the obligate Wnt pathway repressor APC) and Olig1ere:RZfl/fl/mice (Fig. 5H).

Rnf43 regulates OPC Frizzled 1 receptor surface expression

Rnf43 has been reported to regulate Wnt signaling in other organ systems through ubiquitination and altered cell surface presentation of Frizzleds [Koo et al., 2012], the cell membrane receptors for Wnt ligands. Of the Frizzled family of receptors, we found evidence for expression of Fzd1, Fzd2, Fzd6 and Fzd9 protein in OPCs in culture (Fig. 6A). Of these, we found that only Fzd1 was significantly altered in OPCs lacking Rnf43 function. Loss of Rnf43 in Olig1cre:RZfl/fl OPCs leads to significant increases in Fzd1 protein (p=0044, 4.55 fold increase) expression, without detectable increases in Fzd2, 6 or 9, or other Fzd receptors (Fig. 6A–B). Co-immunoprecipitation (Co-IP) on cultured OPCs demonstrated a physical interaction between Fzd1 and Rnf43 (Fig. S7C). Co-transfection of hela cells with vectors expressing a Fzd1-HA fusion protein and either an unfused RNF43-GFP protein or control GFP vector, shows that Rnf43 promotes increased subcellular relocalization of Fzd1 from cell surface to cytoplasm (Fig. 6C–D; p=1.52E-8 Fig. 6d). We also found increased Fzd1 protein expression both in vitro (Fig. 6E) and in vivo (Fig. 6F, Fig. S7D, from 21dpl remyelinating lesions) in NG2-expressing OPCs from Olig1cre:RZfl/fl mice, consistent with Rnf43 targeting the receptor for degradation following internalization from the cell surface [Koo et al., 2012].

Pharmacologic targeting of Frizzled 1 on OPCs promotes remyelination

The requirement for Rnf43 function in remyelination, and its control of OL differentiation through regulation of OPC Fzd1 levels, suggested that pharmacological targeting of Frizzleds might promote myelin regeneration kinetics. UM206 is a synthetic ligand derived from regions of high homology between Wnt3a and Wnt5a that acts to interfere with the interaction between Wnt ligands and Fzd1/2 receptors [Laeremans et al., 2011]. We found that UM206 treatment of wildtype OPCs in culture significantly promoted OPC differentiation compared to vehicle treated controls (Fig. 7A, C; ** p=0.0026, 1.53 fold increase at 2 days and ** p=0.0037, 1.65 fold increase at 3 days). This suggests that untreated wildtype OPCs in vitro experience Wnt stimulation, likely due to the production of Wnt ligands that act autologously, as mentioned above and previously demonstrated [Yuen et al., 2014]. UM206 treatment significantly reversed Wnt3a-induced activation of

Wnt signaling in OPCs (Fig. 7B, marked by *Axin2* or *Notum* mRNA), and reversed the Wnt3a-induced blockade of OPC differentiation (Fig. 7A, C). As UM206 acts to block the Fzd1 receptor upstream of Rnf43 function, we find that UM206 is also able to rescue the phenotype of Rnf43 loss of function in Olig1cre:RZfl/fl OPCs, both in their hypersensitivity to Wnt ligand-induced pathway activation (Fig. 7E), as well as in their diminished potential for differentiation in vitro (Fig. 7D, F). We assessed UM206 effects on remyelination in an ex vivo cerebellar slice culture demyelination paradigm (treatment schematic Fig. S4B). Vehicle treated slice cultures from Olig1cre:RZfl/fl show significant deficits in their ability to remyelinate compared to control slice cultures (Cre negative, RZfl/fl)(Fig. 7G–H), consistent with a function for Rnf43 in OPC differentiation in remyelination. UM206 administration significantly increases the rate of OL differentiation in both wildtype and Olig1cre:RZfl/fl cultures, as evidenced by increased MBP staining along NF200+ axons (Fig. 7G), with near normalization back to untreated wildtype levels in UM206 treated Olig1cre:RZfl/fl (Fig. 7H).

We also assessed UM206 effects on remyelination in vivo in lysolecithin demyelinated lesions in the mouse corpus callosum (treatment schematic Fig. S4C) using osmotic pump delivery of UM206 (schematic Fig. S4D) into the corpus callosum from 3dpl onwards. As previously shown, Olig1cre:RZfl/fl show significant deficits in their ability to remyelinate compared to control animals (Cre negative, RZfl/fl), both in the number of *MAG*+ mRNA expressing OL at 10dpl (Fig. 8A, B), number of remyelinated axons at 14dpl (Fig. 8F) and morphological myelin at 14dpl on EM (Fig. 8G, H). UM206 delivery by osmotic pump from 3dpl until the remyelination endpoint significantly increased the rate of OL differentiation in both wildtype and Olig1cre:RZfl/fl cultures, without any change in total Olig2+ cell number (Fig. 8D, E), as evidenced by increased MAG+ cell number at 10dpl (Fig. 8A, B), and number of remyelinated axons at 14dpl (Fig. 8F) and morphological myelin at 14dpl, with near normalization back to untreated wildtype levels in UM206 treated Olig1cre:RZfl/fl (Fig. 8F–H). Together these results identify a Fzd1 signaling axis as a key regulator of OPC differentiation kinetics in remyelination, and suggest that UM206 can promote remyelination by targeting the interaction of extracellular Wnt ligands with their Frizzled receptors on OPCs.

Discussion

The developmental process of myelination and the regenerative process of remyelination following white matter injury share the common objective of investing axons with myelin sheaths [Fancy et al., 2011a], but evidence for ‘stalled’ oligodendrocyte precursors that fail to engage in remyelination in both MS and human newborn brain injuries [Chang et al., 2002; Wolswijk et al., 1998; Billiards et al., 2008], highlights the importance of understanding OL regulators in the setting of injury [Franklin and Ffrench-Constant, 2017]. Whilst there are clear differences between developmental myelination and remyelination, particularly in terms of the superimposition of inflammation on the regenerative process, the cell intrinsic program of effectors controlling differentiation and maturation in oligodendrocytes has generally been considered to be similar between development and injury, and OL intrinsic factors that may be required only in the setting of injury have been less clear. Here we find that the Ring Finger Protein Rnf43 has critical injury specific

function both in neonatal hypoxic injury and remyelination in the adult, but is dispensable for timely developmental myelination.

Since Rnf43 is a target of Wnt signaling in OPCs, and Wnt signaling is only re-activated in OPCs in the adult in response to injury [Fancy et al., 2009, Fancy et al., 2011b], the presence of RNF43-positive OPCs in adult CNS likely identifies activated cells responding to injury. In line with this, we find Rnf43 expression in OPCs in adult mice only in the context of lesions, and find RNF43 expressing OPCs in human MS lesions, but absence of expression in normal appearing white matter in these same patients. In this respect, RNF43 expression serves as a useful marker to identify the lesion penumbra in MS, where Wnt-activated OPCs are responding to an injury insult. As a Wnt target in OPCs, RNF43 expression also identifies regional differences in Wnt tone in human CNS injury. RNF43 expression in OPCs in human newborn hypoxic ischemic encephalopathy (HIE) exhibits stark differences between white and grey matter, suggesting significant differences in OPC Wnt tone between these different regions. It will be interesting to assess whether such grey/white matter differences in OPC Wnt tone could contribute to the reported differing potential for remyelination between cortical grey matter and underlying white matter lesions in MS [Chang et al., 2012].

Wnt signaling has a number of functions in OPCs in both development and injury, regulating their association with vasculature during perivascular migration [Tsai et al., 2016], regulating tip cell angiogenesis and white matter vascularization [Yuen et al., 2014; Chavali et al., 2020], and acting as a potent inhibitor of further OL differentiation [Fancy et al., 2009; Ye et al., 2009, Feigenson et al., 2009; Fancy et al., 2011b; Fancy et al., 2014; Lee et al., 2015]. Wnt function to block OL differention is mediated by β-catenin in the nucleus, likely in collaboration with Tcf7l2, although Tcf7l2 also appears to be important at later stages for promoting differentiation [Weng et al., 2017] independently of canonical Wnt, perhaps with cofactors such as Groucho or Kaiso. Several studies indicate that, as in other organ systems such as the colonic epithelium, different Wnt functional states can exist in OPCs and that a transition to a higher uncontrolled Wnt state can account for pathological OL differentiation block [Fancy et al., 2014]. A fine balance therefore exists between pathway activators and repressors in OPCs to allow for normal Wnt function whilst preventing transition to this pathological state. Pathway repressors such as Axin2 (a direct target activated by Wnt pathway) and Adenomatous Polyposis Coli (APC) are required in both developmental myelination and remyelination to allow for OL differentiation [Fancy et al., 2011b, Lang et al., 2013; Fancy et al., 2014], and indeed Axin2 can be indirectly pharmacologically targeted via XAV939's effect on the Tankyrase enzyme to promote differentiation kinetics. Another important mechanism for controlling Wnt pathway and allowing OL differentiation in both development and injury is EED (embryonic ectoderm development) mediated histone methylation, that establishes a chromatin landscape that selectively represses inhibitory Wnt [Wang et al., 2020]. Very interestingly this seems to be a mechanism that can also regulate Fzd1 expression levels, amongst other Wnt target genes. Mechanisms such as activation of PPAR gamma and downregulation of Foxg1 can also potentially intersect with and inhibit Wnt pathway [Vallée et al., 2018; Dong et al., 2021], through activation of GSK- 3beta inducing proteasomal β-catenin degradation, and PPAR gamma agonists could serve as promising treatments during demyelinating injury

[Vallée et al., 2018]. Our results indicate that Rnf43 is a potent regulator of the timing of remyelination, an important determinant of functional recovery in human MS and animal models. Whilst the Rnf43 gene serves as a target of Wnt pathway activation both in vitro and during remyelination in vivo, Rnf43 protein acts as a negative feedback mechanism and is required to promote OL differentiation in remyelination through the repression of Wnt signaling in OPCs (Fig. S8). Whilst Wnt signaling negatively regulates OPC differentiation in both development and injury, Rnf43 function comes into play only in the injury response. It is dispensible for timely developmental myelination, but OPCs lacking Rnf43 demonstrate marked delays in OL differentiation and remyelination at 21 days following a demyelinating injury, with fixed deficits in myelin thickness still observable at 50 days after the injury. This recruitment of, and requirement for, a key Wnt repression system in an injury specific context identifies inherent differences in Wnt tone between remyelination and development, and points to an increased propensity for elevated and dysregulated Wnt-induced OL maturation block in adult injury compared to development. Persistent deficits in myelin thickness of remyelinated axons in mice lacking Rnf43 also suggest that a deficient Wnt repressor tone is sufficient for permanent effects on white matter injury repair, and that Wnt repressor tone is a critical factor in determining transition to a pathological Wnt activity state in OPCs.

Rnf43 functions to regulate Wnt pathway in other organ systems, such as the intestinal epithelium, in collaboration with the related Zinc Finger family member Znrf3, and only with simultaneous deletion of both genes do Wnt responsive cells become hypersensitive to the action of extracellular Wnts [Koo et al., 2012, Hao et al., 2012]. Surprisingly, we identify a tissue specific difference in OL lineage in the regulation of these related family members, whereby Znrf3 is neither a target of Wnt pathway nor functions as a repressor of the pathway. Znrf3 is not activated by Wnt pathway in vitro or during remyelination in vivo, and does not contribute to the phenotype seen in the Rnf43/Znrf3 double conditional mutant mouse. Lack of this compensatory mechanism provided by Znrf3 suggests a potential increased propensity for pathway dysregulation in OPCs compared to other Wnt responsive tissues.

Canonical Wnt pathway activation occurs through the binding of extracellular Wnt ligands to the Wnt receptor complex on the surface of cells [Niehrs et el., 2012]. Previous work has demonstrated a mechanism that promotes receptor complex signalosome formation at the OPC surface, via Daam2 association with PIP5K promoting clustering of Wnt receptor complexes into signalosomes through PIP_2 [Lee et al., 2015]. Rnf43 protein functions in opposition of this by regulating the surface availability of the Fzd1 receptor, a receptor for extracellular Wnt ligands (Fig. S8). These opposing mechanisms for toggling ON and OFF Wnt pathway activation at the cell surface may be critical for regulating the Wnt functional states in OPCs in differing conditions of extracellular Wnt ligand availability. The phenotype of dysfunctional remyelination in the absence of Rnf43, and promotion of remyelination by selective pharmacological targeting of Fzd1 using UM206, suggests that paracrine Wnt signals acting on OPCs are critical in actively regulating differentiation kinetics during the normal remyelination process. It will be important to better understand the nature and cellular sources of these Wnt ligands in human injury, and how this may vary

between developmental myelination and remyelination, and between successful and failed remyelination in MS.

STAR Methods

RESOURCE AVAILABILITY

Lead Contact—Further information and requests for resources and reagents should be directed to and will be fulfilled by the lead contact, Stephen Fancy (stephen.fancy@ucsf.edu).

Materials Availability—This study did not generate new unique reagents.

Data and Code Availability

- All data reported in this paper will be shared by the lead contact upon request.
- This paper does not report original code.
- Any additional information required to reanalyze the data reported in this paper is available from the lead contact upon request.

EXPERIMENTAL MODEL AND SUBJECT DETAIL

Mice—Animal husbandry and procedures were performed according to TMMU and UCSF approved protocols. Mouse ages were identified in main text and figure legends. Both mouse genders were used in this study. Mice were randomly assigned to the different experimental groups.

Rnf43 and Znrf3 floxed: These mice have been described previously [Koo et el., 2012]. Through intercrosses with Olig1-cre, Olig2-cre or PDGFRα-creER mice we can achieve conditional knockout of Rnf43/Znrf3 in OPCs. We used a breeding strategy of crossing either Olig1-cre:Rnf43 fl/fl:Znrf3 fl/fl, Olig2-cre:Rnf43 fl/fl:Znrf3 fl/fl or PDGFRα-creER:Rnf43 fl/fl:Znrf3 fl/fl mice with Rnf43 fl/fl:Znrf3 fl/fl mice, thus generating Rnf43/Znrf3 double knock-out offspring and non-cre control littermates.

PDGFRα-creER: These mice have been described previously [Kang et al., 2010]. A tamoxifen inducible cre recombinase gene was inserted into exon 2. These mice were used to cross with Rosa-YFP mice or Rnf43/Znrf3 knock-out mice. In order to induce YFP expression and knock out Rnf43/Znrf3 during remyelination, mice were given tamoxifen (T-5648, Sigma) gavage with 1mg of tamoxifen twice a day for 5 consecutive days (10mg in total).

Olig1-cre and Olig2-cre: These two lines allow for cre mediated activity in oligodendrocyte lineage cells and have been described previously [Arnett et al., 2004; Schüller et al., 2008]. These mice were used to knock-out Rnf43/Znrf3 in OPCs during early development.

APC floxed: These mice have been described previously [Robanus-Maandag et al., 2010]. Olig2-cre:APC fl/fl mice were used to over-activate the Wnt pathway in OPCs.

Human MS and HIE tissues—Human multiple sclerosis post-mortem tissue blocks were provided by the UK Multiple Sclerosis Tissue Bank at Imperial College London. All tissues were collected following fully informed consent by the donors via a prospective donor scheme following ethical approval by the London Multicentre Research Ethics committee (MREC 02/2/39). Multiple sclerosis lesions were characterized as described previously [Lock et al., 2002], using luxol fast blue (LFB) to assess demyelination, SMI-31 immunohistochemistry to assess preservation of axons, and LN3 immunohistochemistry to assess inflammatory cell activity. Lesions with florid parenchymal and perivascular inflammatory cell infiltration, myelin fragmentation, and demyelination with indistinct margins were classified as active plaques. Areas of normal appearing white matter 'NAWM' from each patient were also assessed.

All human HIE tissue was collected with informed consent and in accordance with guidelines established by UCSF Committee on Human Research (H11170-19113-07) as previously described [Fancy et al., 2011b]. Immediately after procurement, all brains were immersed in PBS with 4% paraformaldehyde for 3 d. On day 3, the brain was cut in the coronal plane at the level of the mammillary body and immersed in fresh 4% paraformaldehyde and PBS for an additional 3 d. After fixation, all tissue samples were equilibrated in PBS with 30% sucrose for at least 2 d. After sucrose equilibration, tissue was placed into molds and embedded with optimal cutting temperature medium for 30 min at room temperature followed by freezing in dry ice–chilled ethanol. UCSF neuropathology staff performed brain dissection and its evaluation. The diagnosis of HIE requires clinical and pathological correlation; no widely accepted diagnostic criteria are present for the pathological diagnosis of HIE. None of the HIE cases evaluated in this study were identical, but they did show consistent evidence of diffuse white matter gliosis, as evaluated by the qualitative increase in the number of GFAP-positive cells in addition to the increased intensity of GFAP staining.

Lysolecithin lesioning—This method has been described previously [Niu et al., 2019]. Demyelinated lesions were produced in the corpus callosum white matter of 8-week-old mice and littermate control mice. Anesthesia was induced and maintained with inhalational isoflurane and oxygen supplemented with 0.05 ml of buprenorphine (Vetergesic; 0.05 mg/ml) given subcutaneously. After exposing the brain at the level of 1.0 mm rostral, 1.0 mm lateral and 1.9 mm ventral to bregma, 1 μl 1% lysolecithin (L-α-lysophosphatidylcholine) was injected into the white matter, and the needle was left in place for 5 min following injection to reduce backflow.

Murine chronic neonatal hypoxia—This method has been described previously [Cree et al., 2018]. Mice pups with their parents were subjected to chronic sublethal hypoxia starting at P3, receiving chronic neonatal hypoxaemia (10% fraction of inspired oxygen). At P10, those hypoxic mice brain tissues were collected and compared to that of normoxic mice. At least four mice per group, for each of the transgenic mice and for the two groups normoxia versus hypoxia, were collected at P10. All animal husbandry and procedures were performed according to UCSF guidelines under IACUC approved protocols.

METHOD DETAILS

Immunohistochemistry—Mice of different ages were anesthetized and transcardially perfused with 4% paraformaldehyde. Brains were dissected and cryoprotected in 30% sucrose. Serial coronal sections were obtained using a cryostat microtome. For immunostaining, these brain sections were blocked with 0.5% bovine serum albumin and 0.2% triton X-100 for 1 hour at room temperature, followed by an incubation with primary antibodies overnight at 4°C.

Primary antibodies were to the following proteins: PDGFRα (1:200, rat, 558774, BD Biosciences), PDGFRα (1:8000, rabbit, gift from W. Stallcup, Sanford Burnham Prebys), Olig2 (1:2000, rabbit, gift from C.D. Stiles, Harvard), RNF43 (1:200, rabbit, ab84125, Abcam), NF200 (1:1000, rabbit, N4142, Sigma), Rnf43 (1:200, rabbit, ab217787, Abcam), FZD1 (1:200, Rat, MAB11201, R&D), MBP (1:500, rat, MCA409S, Serotec), NG2 (1:200, mouse, 05-710, Millipore), HA (1:200, mouse, AH158, Beyotime), Ki67 (1:1000, rabbit, MA5-14520, Thermo Fisher Scientific), Olig2 (1:200, mouse, MABN50, Millipore). Appropriate Alexa-Fluor-conjugated secondary antibodies (1:1000, Life Technologies) were used to visualize the primary antibodies. Cell counting and fluorescence intensity analyses were conducted on nine randomly chosen fields of cell cultures or fixed areas of brains using an Image Pro Plus image analysis system. The method has also been described previously [Arnett et al., 2004].

In Situ Hybridization—Brain and spinal cord tissues were collected as described above and cryoprotected in 30% sucrose with 0.1% diethyl pyrocarbonate. Serial coronal or transverse sections were obtained using a cryostat microtome. For in situ hybridization staining, sections were incubated with diluted denatured antisense probes at 65°C overnight, followed by three 65°C post-hybridization washes and two room temperature washes, and then were incubated with anti-Digoxigenin-AP Fab fragments antibody (1:1500, 11093274910, Sigma-Aldrich) at 4°C overnight. DIG labeled antisense MAG and PLP-DM20 probes were used to target mature oligodendrocytes. The targeted mRNA-expressing cells were visualized as a dark purple deposition with NBT/BCIP–alkaline phosphatase combination (11681451001, Sigma-Aldrich) the following day. Cell counting was performed under a 10× objective lens for each sample using an Image Pro Plus software. The technique has also been described previously [Niu et al., 2019].

OPC culture—Mouse OPCs were isolated by immunopanning from P8 mouse cortices. Panning dishes were incubated with secondary and primary antibodies sequentially. Mouse brain cerebral hemispheres were minced and dissociated with papain at 37°C for 60 min. After trituration, cells were resuspended in a panning buffer and then incubated at room temperature sequentially on three immunopanning dishes: Ran-2, GalC, and O4. O4 positive mouse OPCs were released from the final panning dish by 0.05% trypsin (Invitrogen). These purified mouse OPCs were cultured in poly-D-lysine-coated 10 cm dishes or 24-well plates with cover slips for experiments. In the OPC culture medium, PDGF-AA (10ng/ml, 100-13A, Peprotech) was used to stimulate OPC proliferation and was removed from culture medium to induce OPC differentiation. The cells were collected for OPC membrane protein

extraction and Western blot. Cells on cover slips were fixed for immunohistochemistry. The technique has also been described previously [Mei et al., 2014].

Cerebellar slice culture—For the cerebellar slice cultures. P3 mouse brains were dissected out into pre-cold ACSF. Cerebellar slices (300 μm thick) were cut on a vibroslicer (Leica VT 1000S, Wetzlar, Germany) and transferred to the Millicell-CM organotypic culture inserts (Millipore, 0.4 μm) with DMEM slice culture medium containing 25% heat-inactivated horse serum, 25% HBSS, 1% N2 and penicillin-streptomycin. Slices were cultured at 37 °C and 7.5% CO2 for 10 days, and then demyelination induced by the addition of 0.5% lysolecithin (Sigma) to the slice culture medium for 18 h. Following demyelination, slices were then transferred to a new plate with culture medium with or without UM206, and cultured for an additional 10 days to allow remyelination to occur.

Osmotic pump delivery of UM206—Osmotic pumps and catheters were purchased from ALZET (0004317 micro-osmotic pump model 1002; 0008851 brain infusion kit 3, 1-3 mm) to deliver 0.25μl UM206 per hour directly into the mouse corpus callosum at 3 dpl. Briefly, the osmotic pump was connected to the catheter, filled with 200 μl of saline spiked with or without UM206 (1 mg/1.5 ml concentration), then implanted subcutaneously following the manufacturer's instructions (ALZET). At 10 dpl or 14 dpl, the pump was removed after the mouse was transcardially perfused with 4% formaldehyde.

Plasmids and electroporation—HA-fusion expressed FZD1 plasmid (FZD1-HA) and GFP-infusion expressed Rnf43 plasmid (Rnf43-GFP) were generated by PCR-subcloning. Plasmid vectors (FZD1-HA + GFP or FZD1-HA + Rnf43-GFP) were cotransfected into the Hela cell line using Amaxa Nucleofector Kit (Lonza) according to the manufacturer's instructions.

Western blot—Western blot was used to quantify differential FZD membrane expression levels in OPCs. OPC membrane protein samples were extracted from cultured non-cre control OPCs (fl/fl) and Olig1-cre:Rnf43 fl/fl:Znrf3 fl/fl double knock-out OPCs (Olig1-cre:RZ fl/fl) according to the Mem-PER™ Plus Membrane Protein Extraction Kit instruction (89842, ThermoFisher). Protein samples were separated on 10% SDS-PAGE gels, transferred to nitrocellulose membranes and probed with antibody against FZD1 (1:500, rat, MAB11201, R&D), FZD2 (1:1000, goat, PA5-47119, Invitrogen), FZD3 (1:500, goat, AF1001, R&D), FZD4 (1:500, rat, MAB194, R&D), FZD5 (1:500, rabbit, ab75234, Abcam), FZD6 (1:500, mouse, sc-393791, Santa Cruz), FZD7 (1:500, rabbit, NBP2-23624, Novus Biologicals), FZD8 (1:500, rabbit, NLS4767, Novus Biologicals), FZD9 (1:500, goat, AF2440, R&D), and FZD10 (1:500, rabbit, ab83044, Abcam). Na-K-ATPase was used as loading control (1:1000, Rabbit, #3010, Cell signaling technology). Protein bands were visualized by chemiluminescence (ECL Plus, GE Healthcare) after incubation with HRP-conjugated secondary antibodies. Protein band intensity was analyzed using the Image Pro Plus software as previously described [Niu et al., 2019].

qPCR—Total ribonucleic acid (RNA) was isolated using RNeasy Plus Mini Kit (74134, Qiagen). Quantitative polymerase chain reaction (qPCR) was performed with the C1000 Touch™ Real-time PCR Detection System (Bio-Rad) and GoTaq® qPCR Master Mix

(Promega). The oligonucleotide primers, amplification procedure, and melt curve analysis were performed. For each sample, independent repeats were performed in triplicate.

Co-Immunoprecipitation—Co-immunoprecipitation (Co-IP) was performed on cultured OPCs using target Rnf43-specific antibody to pulldown FZD1 protein. Briefly, OPC lysates extracted with RIPA buffer were incubated with anti-Rnf43 antibody (1:100, PA5-79930, Invitrogen), or normal IgG antibody (1:200, 2729S, CST, negative control) at 4°C overnight, followed by incubation with protein A/G beads (sc-2003, Santa Cruz) at 4°C for 4 h. The immunocomplexes were washed 5 times with lysis buffer, eluted in ×1.5 sample buffer, then examined by immunoblotting with anti-FZD1 antibody (1:1000, PA5-47072, Invitrogen). The OPC lysate sample without IP (Input) was used as positive control for indicating the position of FZD1 band.

Electron microscopy—As previously described [Cree et al., 2018], mice were anesthetized and perfused trans-cardially with 4% glutaraldehyde and postfixed overnight. Samples were stained with osmium tetroxide overnight and dehydrated in a series of ethanol dehydration treatments. Embedding was performed in TAAB resin. Sections were cut at 1-μm intervals and stained with toluidine blue for identifying lesion sites. More than 200 axons in developmental tissues and within lesion sites were examined using electron microscopy. The myelinated axon numbers and G-ratios were calculated to assess myelination and remyelination.

QUANTIFICATIONS AND STATISTICAL ANALYSIS

Quantifications—To quantify positive cell numbers, cell counting was conducted on nine randomly chosen fields for each sample using an Image Pro Plus image analysis system. To quantify fluorescent positive area, the immunofluorescent signal was determined using a fluorescence microscope (Zeiss) or a confocal laser-scanning microscope (Olympus, FV3000) with excitation wavelengths appropriate for Alexa Fluor 488 (488 nm, Life Technologies), Alexa Fluor 568 (568 nm) or Alexa Fluor 647 (647 nm). Fluorescent intensity and Western-blot positive band, the positive areas were automatically selected in image-Pro Plus 5 software. The areas of interest (AOI) were separated by setting threshold at least two times the background. Cell counting and fluorescence intensity analyses were conducted on six randomly chosen fields for each sample using an Image Pro Plus image analysis system.

Statistical analysis—Statistical significance between groups was determined with GraphPad Prism software. The unpaired t-test was used to determine the significance between two experimental groups. One-way analysis of variance (ANOVA) was used to determine the significances among three and four groups. A probability of $P<0.05$ was considered statistically significant. All significant statistical results are indicated within the figures with the following conventions: * $P < 0.05$, ** $P < 0.01$, *** $P < 0.001$, **** $P < 0.0001$. Error bars represent ± s.d. No statistical methods were used to pre-determine sample sizes but our sample sizes are similar to those reported in previous publications [Niu et al., 2019]. Data distribution was assumed to be normal, but this was not formally tested. All

experiments were performed at least 3 times, and the findings were replicated in individual mice and cell cultures in each experiment.

Supplementary Material

Refer to Web version on PubMed Central for supplementary material.

Acknowledgments

We would like to thank Hans Clevers (Hubrecht Institute) for providing us with Rnf43 floxed and Znrf3 floxed mouse lines. This work was supported by grants from the National Key Research and Development Program of China (2017YFA0106000), National Nature Science Foundation of China (31871045, 32070964) to J.N., and NIH/NINDS (R01NS097551, P01NS083513, R21NS119954) to S.P.J.F. S.P.J.F. is a Harry Weaver Neuroscience Scholar of the National Multiple Sclerosis Society.

References:

Arnett HA, Fancy SP, Alberta JA, Zhao C, Plant SR, Kaing S, Raine CS, Rowitch DH, Franklin RJ, Stiles CD. (2004). bHLH transcription factor Olig1 is required to repair demyelinated lesions in the CNS. Science. 306(5704):2111–5. [PubMed: 15604411]

Billiards SS, Haynes RL, Folkerth RD, Borenstein NS, Trachtenberg FL, Rowitch DH, Ligon KL, Volpe JJ, Kinney HC. (2008). Myelin abnormalities without oligodendrocyte loss in periventricular leukomalacia. Brain Pathol. 18(2): 153–63. [PubMed: 18177464]

Chang A, Tourtellotte WW, Rudick R, Trapp BD. (2002). Premyelinating oligodendrocytes in chronic lesions of multiple sclerosis. N Engl J Med. 346(3): 165–73. [PubMed: 11796850]

Chang A, Staugaitis SM, Dutta R, Batt CE, Easley KE, Chomyk AM, Yong VW, Fox RJ, Kidd GJ, Trapp BD. (2012). Cortical remyelination: a new target for repair therapies in multiple sclerosis. Ann Neurol. 72(6):918–26. [PubMed: 23076662]

Chavali M, Ulloa-Navas MJ, Pérez-Borredá P, Garcia-Verdugo JM, McQuillen PS, Huang EJ, Rowitch DH. (2020). Wnt-Dependent Oligodendroglial-Endothelial Interactions Regulate White Matter Vascularization and Attenuate Injury. Neuron. 108(6):1130–1145. [PubMed: 33086038]

Clevers H (2006). Wnt/beta-catenin signaling in development and disease. Cell. 127(3): p. 469–80. [PubMed: 17081971]

Cree BAC, Niu J, Hoi KK, Zhao C, Caganap SD, Henry RG, Dao DQ, Zollinger DR, Mei F, Shen YA, Franklin RJM, Lillian EM, Xiao L, Chan JR, Fancy SPJ. (2018). Clemastine rescues myelination defects and promotes functional recovery in hypoxic brain injury. Brain. 141(1):85–98. [PubMed: 29244098]

Dong F, Liu D, Jiang F, Liu Y, Wu X, Qu X, Liu J, Chen Y, Fan H, Yao R. (2021). Conditional Deletion of Foxg1 Alleviates Demyelination and Facilitates Remyelination via the Wnt Signaling Pathway in Cuprizone-lnduced Demyelinated Mice. Neurosci Bull. 37(1): 15–30. [PubMed: 33015737]

Fancy SP, Baranzini SE, Zhao C, Yuk DI, Irvine KA, Kaing S, Sanai N, Franklin RJ, Rowitch DH. (2009). Dysregulation of the Wnt pathway inhibits timely myelination and remyelination in the mammalian CNS. Genes and Development. 23(13):1571–85. [PubMed: 19515974]

Fancy SP, Chan JR, Baranzini SE, Franklin RJ, Rowitch DH. (2011a). Myelin Regeneration – A Recapitulation of Development? Annual Reviews Neuroscience. 34:21–43.

Fancy SP, Harrington EP, Yuen TJ, Silbereis JC, Zhao C, Baranzini SE, Bruce CC, Otero JJ, Huang EJ, Nusse R, Franklin RJ, Rowitch DH. (2011b). Axin2 as regulatory and therapeutic target in newborn brain injury and remyelination. Nat Neuroscience. 14(8): 1009–16. [PubMed: 21706018]

Fancy SP, Harrington EP, Baranzini SE, Silbereis JC, Shiow LR, Yuen TJ, Huang EJ, Lomvardas S, Rowitch DH. (2014). Parallel states of pathological Wnt signaling in neonatal brain injury and colon cancer. Nature Neuroscience. 17(4):506–12. [PubMed: 24609463]

Franklin RJM, Ffrench-Constant C. (2017). Regenerating_CNS_myelin_- from mechanisms to experimental medicines. Nat Rev Neurosci. 18(12):753–769. [PubMed: 29142295]

Gallo V, Deneen B. (2014). Glial development: the crossroads of regeneration and repair in the CNS. Neuron. 83(2):283–308. [PubMed: 25033178]

Hao HX, Xie Y, Zhang Y, Charlat O, Oster E, Avello M, Lei H, Mickanin C, Liu D, Ruffner H, Mao X, Ma Q, Zamponi R, Bouwmeester T, Finan PM, Kirschner MW, Porter JA, Serluca FC, Cong F. (2012). ZNRF3 promotes Wnt receptor turnover in an R-spondin-sensitive manner. Nature. 485(7397):195–200. [PubMed: 22575959]

Jung M, Krämer E, Grzenkowski M, Tang K, Blakemore W, Aguzzi A, Khazaie K, Chlichlia K, von Blankenfeld G, Kettenmann H, et al. (1995). Lines of murine oligodendroglial precursor cells immortalized by an activated neu tyrosine kinase show distinct degrees of interaction with axons in vitro and in vivo. Eur J Neurosci. 7(6):1245–65. [PubMed: 7582098]

Kang SH, Fukaya M, Yang JK, Rothstein JD, Bergles DE. (2010). NG2+ CNS glial progenitors remain committed to the oligodendrocyte lineage in postnatal life and following neurodegeneration. Neuron. 68(4):668–81. [PubMed: 21092857]

Koo BK, Spit M, Jordens I, Low TY, Stange DE, van de Wetering M, van Es JH, Mohammed S, Heck AJ, Maurice MM, Clevers H. (2012). Tumour suppressor RNF43 is a stem-cell E3 ligase that induces endocytosis of Wnt receptors. Nature. 488(7413): 665–9. [PubMed: 22895187]

Kucharova K, Chang Y, Boor A, Yong VW, Stallcup WB. (2011). Reduced inflammation accompanies diminished myelin damage and repair in the NG2 null mouse spinal cord. J Neuroinflammation. 8:158. [PubMed: 22078261]

Laeremans H, Hackeng TM, van Zandvoort MA, Thijssen VL, Janssen BJ, Ottenheijm HC, Smits JF, Blankesteijn WM. (2011). Blocking of frizzled signaling with a homologous peptide fragment of wnt3a/wnt5a reduces infarct expansion and prevents the development of heart failure after myocardial infarction. Circulation. 124(15):1626–35. [PubMed: 21931076]

Lang J, Maeda Y, Bannerman P, Xu J, Horiuchi M, Pleasure D, Guo F. (2013). Adenomatous polyposis coli regulates oligodendroglial development. J Neurosci. 33(7):3113–30. [PubMed: 23407966]

Lee HK, Chaboub LS, Zhu W, Zollinger D, Rasband MN, Fancy SP, Deneen B. (2015). Daam2-PIP5K is a regulatory pathway for Wnt signaling and therapeutic target for remyelination in the CNS. Neuron. 85(6):1227–43. [PubMed: 25754822]

Lock C, Hermans G, Pedotti R, Brendolan A, Schadt E, Garren H, Langer-Gould A, Strober S, Cannella B, Allard J, Klonowski P, Austin A, Lad N, Kaminski N, Galli SJ, Oksenberg JR, Raine CS, Heller R, Steinman L. (2002). Gene-microarray analysis of multiple sclerosis lesions yields new targets validated in autoimmune encephalomyelitis. Nature Medicine. 8(5): 500–8.

Mei F, Fancy SPJ, Shen YA, Niu J, Zhao C, Presley B, Miao E, Lee S, Mayoral SR, Redmond SA, Etxeberria A, Xiao L, Franklin RJM, Green A, Hauser SL, Chan JR. (2014). Fabricated micropillar arrays as a novel high-throughput screening platform for potential therapeutics in Multiple Sclerosis. Nature Medicine. 20(8):954–960.

Niehrs C (2012). The complex world of WNT receptor signalling. Nat Rev Mol Cell Biol. 13(12):767–79. [PubMed: 23151663]

Niu J, Tsai HH, Hoi KK, Huang N, Yu G, Kim K, Baranzini SE, Xiao L, Chan JR, Fancy SPJ. (2019). Aberrant oligodendroglial-vascular interactions disrupt the Blood Brain Barrier triggering CNS inflammation. Nature Neuroscience. 22(5):709–718. [PubMed: 30988524]

Planas-Paz L, Orsini V, Boulter L, Calabrese D, Pikiolek M, Nigsch F, Xie Y, Roma G, Donovan A, Marti P, Beckmann N, Dill MT, Carbone W, Bergling S, Isken A, Mueller M, Kinzel B, Yang Y, Mao X, Nicholson TB, Zamponi R, Capodieci P, Valdez R, Rivera D, Loew A, Ukomadu C, Terracciano LM, Bouwmeester T, Cong F, Heim MH, Forbes SJ, Ruffner H, Tchorz JS. (2016). The RSPO-LGR4/5-ZNRF3/RNF43 module controls liver zonation and size. Nat Cell Biol. 18(5):467–79. [PubMed: 27088858]

Reich DS, Lucchinetti CF, Calabresi PA. (2018) Multiple Sclerosis. N Engl J Med. 378(2):169–180. [PubMed: 29320652]

Robanus-Maandag EC, Koelink PJ, Breukel C, Salvatori DC, Jagmohan-Changur SC, Bosch CA, Verspaget HW, Devilee P, Fodde R, Smits R. (2010). A new conditional Ape-mutant mouse model for colorectal cancer. Carcinogenesis. 31(5):946–52. [PubMed: 20176656]

Schüller U, Heine VM, Mao J, Kho AT, Dillon AK, Han YG, Huillard E, Sun T, Ligon AH, Qian Y, Ma Q, Alvarez-Buylla A, McMahon AP, Rowitch DH, Ligon KL. (2008). Acquisition of

granule neuron precursor identity is a critical determinant of progenitor cell competence to form Shh-induced medulloblastoma. Cancer Cell. 14(2):123–34. [PubMed: 18691547]

Silbereis JC, Huang EJ, Back SA, Rowitch DH. (2010). Towards improved animal models of neonatal white matter injury associated with cerebral palsy. Dis Model Mech. 3(11–12):678–88. [PubMed: 21030421]

Szenker-Ravi E, Altunoglu U, Leushacke M, Bosso-Lefèvre C, Khatoo M, Thi Tran H, Naert T, Noelanders R, Hajamohideen A, Beneteau C, de Sousa SB, Karaman B, Latypova X, Ba§aran S, Yücel EB, Tan TT, Vlaminck L, Nayak SS, Shukla A, Girisha KM, Le Caignec C, Soshnikova N, Uyguner ZO, Vleminckx K, Barker N, Kayserili H, Reversade B. (2018). RSP02 inhibition of RNF43 and ZNRF3 governs limb development independently of LGR4/5/6. Nature. 557(7706):564–569. [PubMed: 29769720]

Tsai HH, Niu J, Munji R, Davalos D, Chang J, Zhang H, Tien AC, Kuo CJ, Chan JR, Daneman R, Fancy SP. (2016). Oligodendrocyte precursors migrate along vasculature in the developing nervous system. Science. 2016. 351(6271):379–84. [PubMed: 26798014]

Vallée A, Vallée JN, Guillevin R, Lecarpentier Y. (2018). Interactions Between the Canonical WNT/Beta-Catenin Pathway and PPAR Gamma on Neuroinflammation, Demyelination, and Remyelination in Multiple Sclerosis. Cell Mol Neurobiol. 38(4):783–795. [PubMed: 28905149]

Volpe JJ. (2009). Brain injury in premature infants: a complex amalgam of destructive and developmental disturbances. Lancet Neurol. 8(1): 110–124. [PubMed: 19081519]

Wang J, Yang L, Dong C, Wang J, Xu L, Qiu Y, Weng Q, Zhao C, Xin M, Lu QR. (2020). EED-mediated histone methylation is critical for CNS myelination and remyelination by inhibiting WNT, BMP, and senescence pathways. Sci Adv. 6(33):eaaz6477. [PubMed: 32851157]

Weng C, Ding M, Fan S, Cao Q, Lu Z. (2017). Transcription factor 7 like 2 promotes oligodendrocyte differentiation and remyelination. Mol Med Rep. 16(2):1864–1870. [PubMed: 28656232]

Wolswijk G (1998). Chronic stage multiple sclerosis lesions contain a relatively quiescent population of oligodendrocyte precursor cells. J Neurosci. 18(2): 601–9. [PubMed: 9425002]

Ye F, Chen Y, Hoang T, Montgomery RL, Zhao XH, Bu H, Hu T, Taketo MM, van Es JH, Clevers H, Hsieh J, Bassel-Duby R, Olson EN, Lu QR. (2009). HDAC1 and HDAC2 regulate oligodendrocyte differentiation by disrupting the beta-catenin-TCF interaction. Nat Neuroscience. 12(7): 829–38. [PubMed: 19503085]

Yuen TJ, Silbereis JC, Griveau A, Chang SM, Daneman R, Fancy SPJ, Zahed H, Maltepe E, Rowitch DH. (2014). Oligodendrocyte-Encoded HIF Function couples postnatal Myelination and White Matter Angiogenesis. Cell. 158, 383–396. [PubMed: 25018103]

Highlights

1. RNF43 marks activated OPCs in human white matter injury.
2. Rnf43 is required for OPC differentiation in injury, not in development.
3. Rnf43 inhibits Wnt pathway by regulating Fzd1 surface presentation on OPCs.
4. Pharmacological inhibition of Fzd1 promotes OPC differentiation during remyelination.

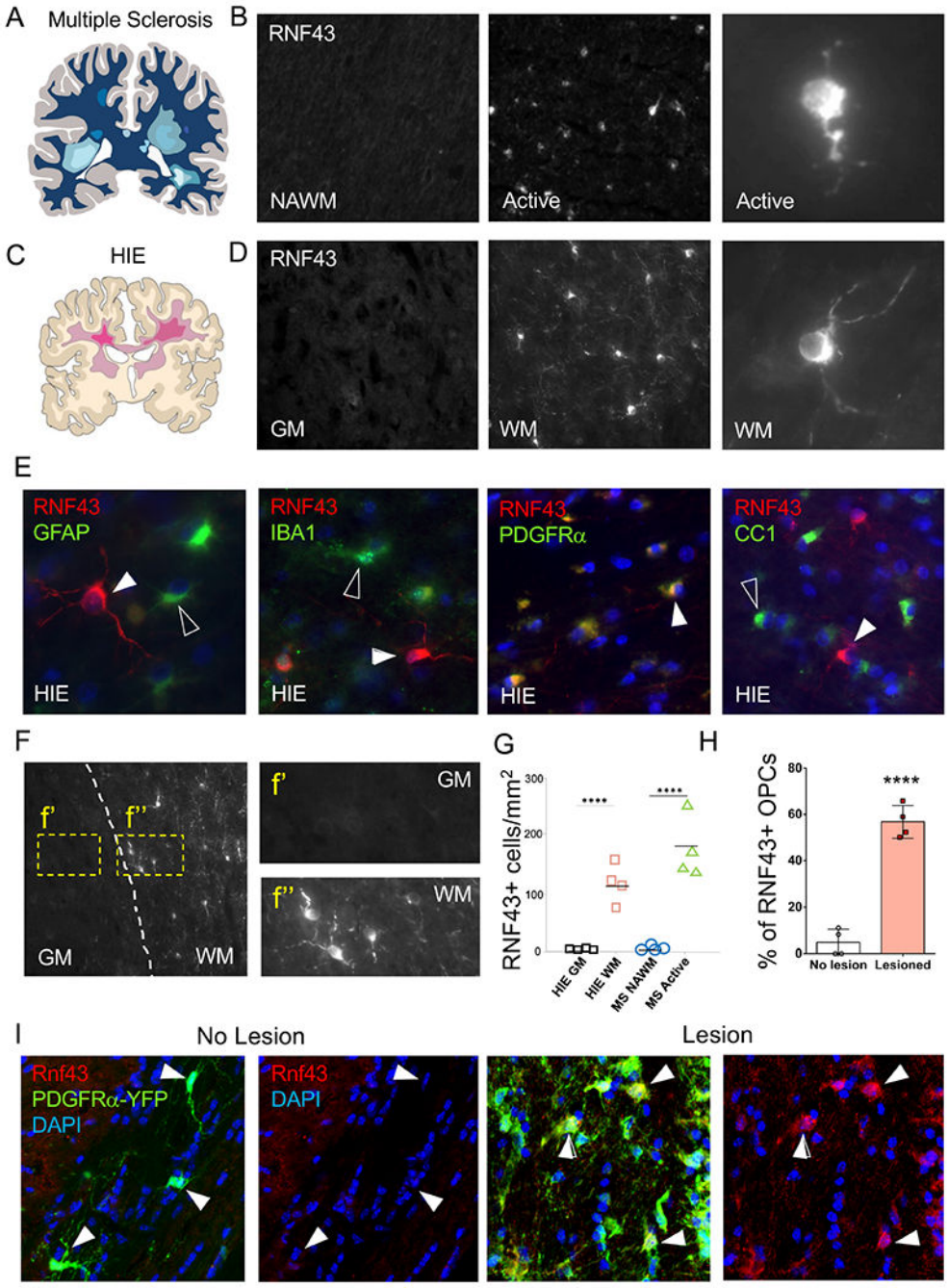

Fig. 1: Rnf43 identifies OPCs in human and mouse white matter injury.

(A, B) RNF43 protein expression identifies OPCs in MS Active lesions (Active), but expression is not seen in surrounding Normal Appearing white Matter (NAWM) from the same cases. (C, D) RNF43 protein is expressed in OPCs in white matter (WM) in the neonatal human white matter injury HIE but is not seen in grey matter (GM) in those same cases. (E) RNF43 expression in red (white arrowheads) colocalizes with the OPC marker PDGFRα in human HIE WM, but separates from markers of other cell types (unfilled arrowheads) such as astrocytes (GFAP), microglia (IBA1), and also from mature

oligodendrocytes (CC1) (quantification in Fig. S1G). (F) Staining for RNF43 protein at the boundary of grey (GM) versus white (WM) matter in human HIE (with boxed enlargements shown in f' and f' to the right). (G) Quantification of RNF43+ OPCs in MS active lesions and NAWM (n= 4 cases) and human HIE GM versus WM (n=4 cases). (H, I) Rnf43 expression is not seen in mouse adult uninjured CNS, but is expressed in OPCs during remyelination. (I) Rnf43 protein (red) and YFP (green) in PDGFRα-YFP transgenic mice (in which OPCs are labelled with YFP), showing lack of any Rnf43 expression in uninjured CNS ('No lesion'), but significant expression in OPCs in a 3dpl corpus callosum lesion following lysolecithin induced demyelination, with quantification in (H)(n=4 animals). See also Fig. S1.

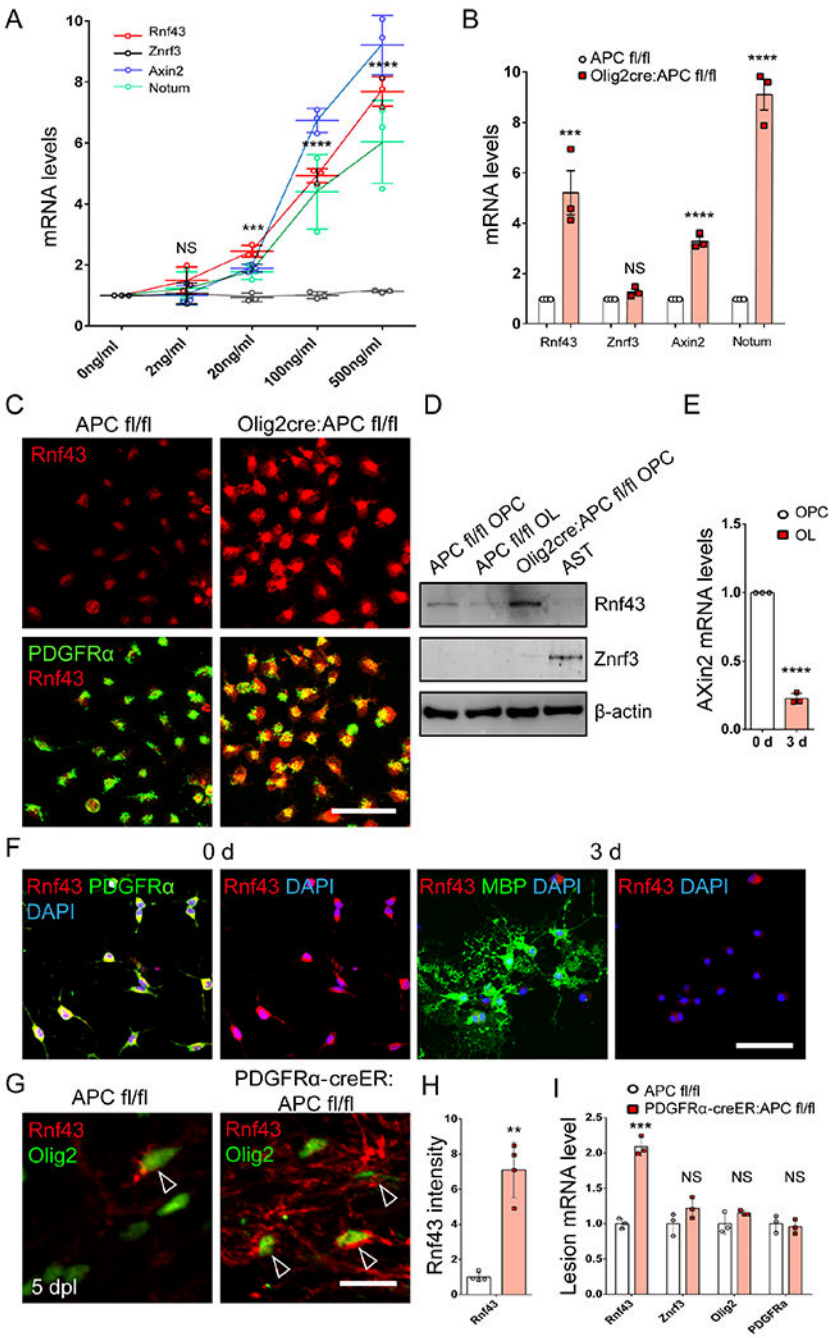

Fig. 2: Rnf43, but not Znrf3, is a target of Wnt in OPCs.

(A) Fold change of mRNA levels for *Rnf43, Znrf3, Axin2* and *Notum* in cultured wildtype OPCs treated with varying concentrations of Wnt3a (marked on x axis) compared to no treatment (n=3 independent experiments). (B) Fold change of mRNA levels for *Rnf43, Znrf3, Axin2* and *Notum* in cultured OPCs derived from Olig2cre:APCfl/fl mice compared to control APC fl/fl/mice (n=3 independent experiments. (C) Rnf43 immunohistochemistry (and co-staining with Pdgfrα) in cultured OPCs derived from Olig2cre:APCfl/fl mice compared to control APCfl/fl mice. Scale bar 50μm. (D) Protein levels by western blot

of Rnf43 and Znrf3 in cultured OPCs, differentiated OL, and astrocytes (AST) from control APCfl/fl mice and in OPCs from Olig2cre:APCfl/fl mice. (E) Fold change of *Rnf43* mRNA in cultured wildtype OPCs versus mature OL differentiated for 3 days (n=3 independent experiments). (F) Rnf43 immunohistochemistry in cultured PDGFRα expressing WT OPCs, and in differentiated OL expressing MBP after 3 days of switching to differentiation media. (G) Rnf43 protein fluorescent intensity is significantly increased in Olig2+ OPCs (arrowheads) from PDGFRα-creER:APC fl/fl mice compared to APC fl/fl control (non cre) mice at 5dpl following lysolecithin induced corpus callosum focal demyelination (Scale bar 20μ), with Rnf43 fluorescent intensity quantification in OPCs in (H). (I) Fold changes of total mRNA levels in 5dpl lesioned corpus callosum tissues of PDGFRα-creER:APC fl/fl mice compared to APC fl/fl control. Values in all panels are mean±s.d. NS not significant, *p<0.05, ** p<0.01, *** p<0.001, **** p<0.0001.

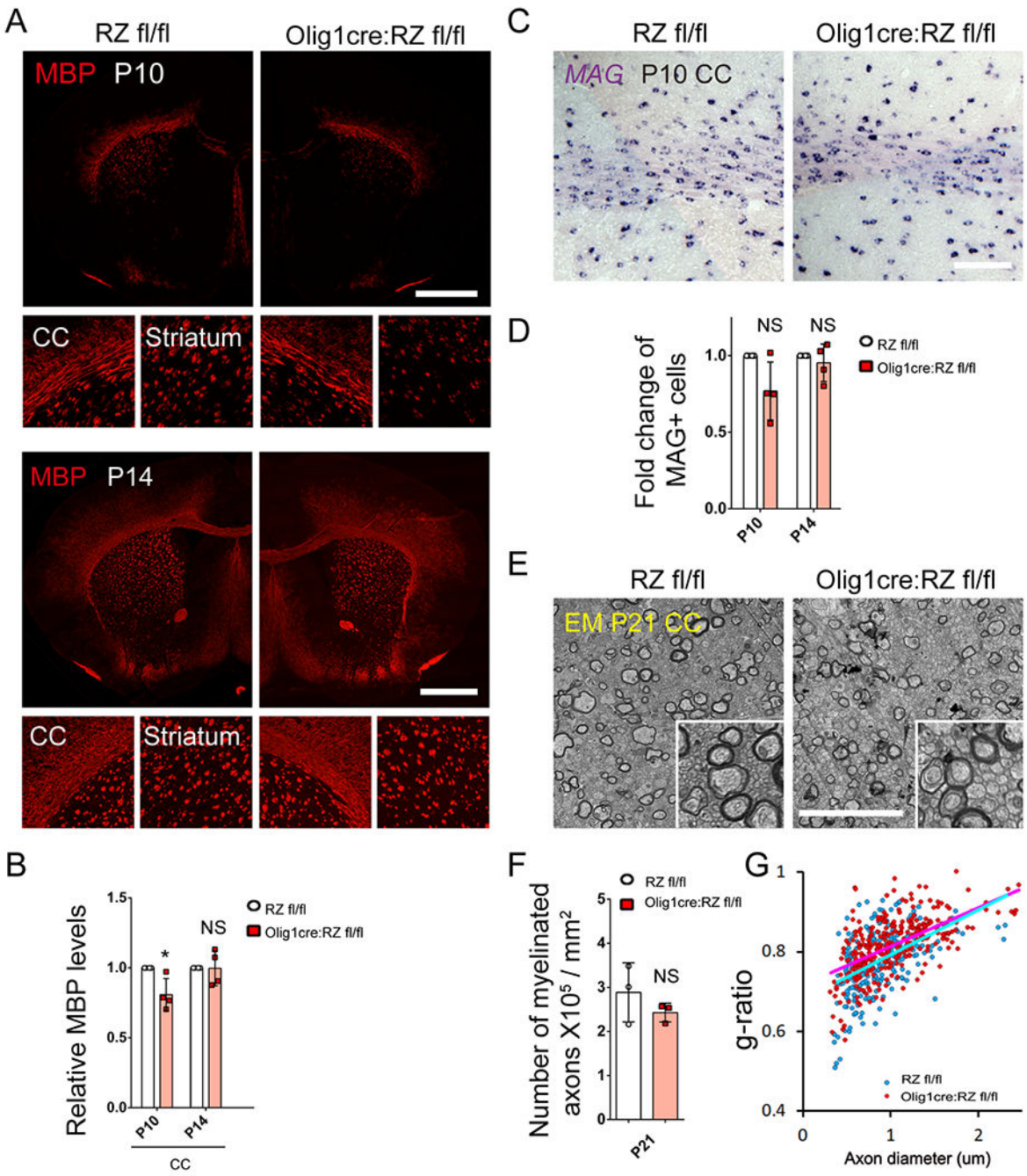

Fig. 3: Rnf43 and Znrf3 functions are dispensable for developmental myelination

(A) MBP immunohistochemistry in multiple brain regions at postnatal day 10 (P10) and P14 in Olig1cre:RZ fl/fl (double Rnf43/Znrf3 floxed mice referred to as RZfl/fl) and RZfl/fl control (non cre) mice brains. Scale bar 1mm. (B) Fold change of MBP fluorescent intensities at P10 and P14 in Olig1cre:RZ fl/fl corpus callosum (CC) compared to RZfl/fl control (n=4 animals). (C, D) *MAG+* mRNA expressing mature OL by in situ hybridization (C), and quantification of fold change (D)(n=4 animals), in Olig1cre:RZ fl/fl CC compared to RZfl/fl control. (E, F, G) Electron-microscopy (EM)(E), quantification of number of

myelinated axons (F), and G-ratio calculations of myelinated axons (G) in P21 CC of RZfl/fl control and Olig1cre:RZ fl/fl. Scale bar 10μ in E. n=3 animals; The scatterplot in (G) displays g-ratios of individual axons as a function of axonal diameter. Values in all panels are mean±s.d. NS not significant, *p<0.05. See also Fig. S2 and S3.

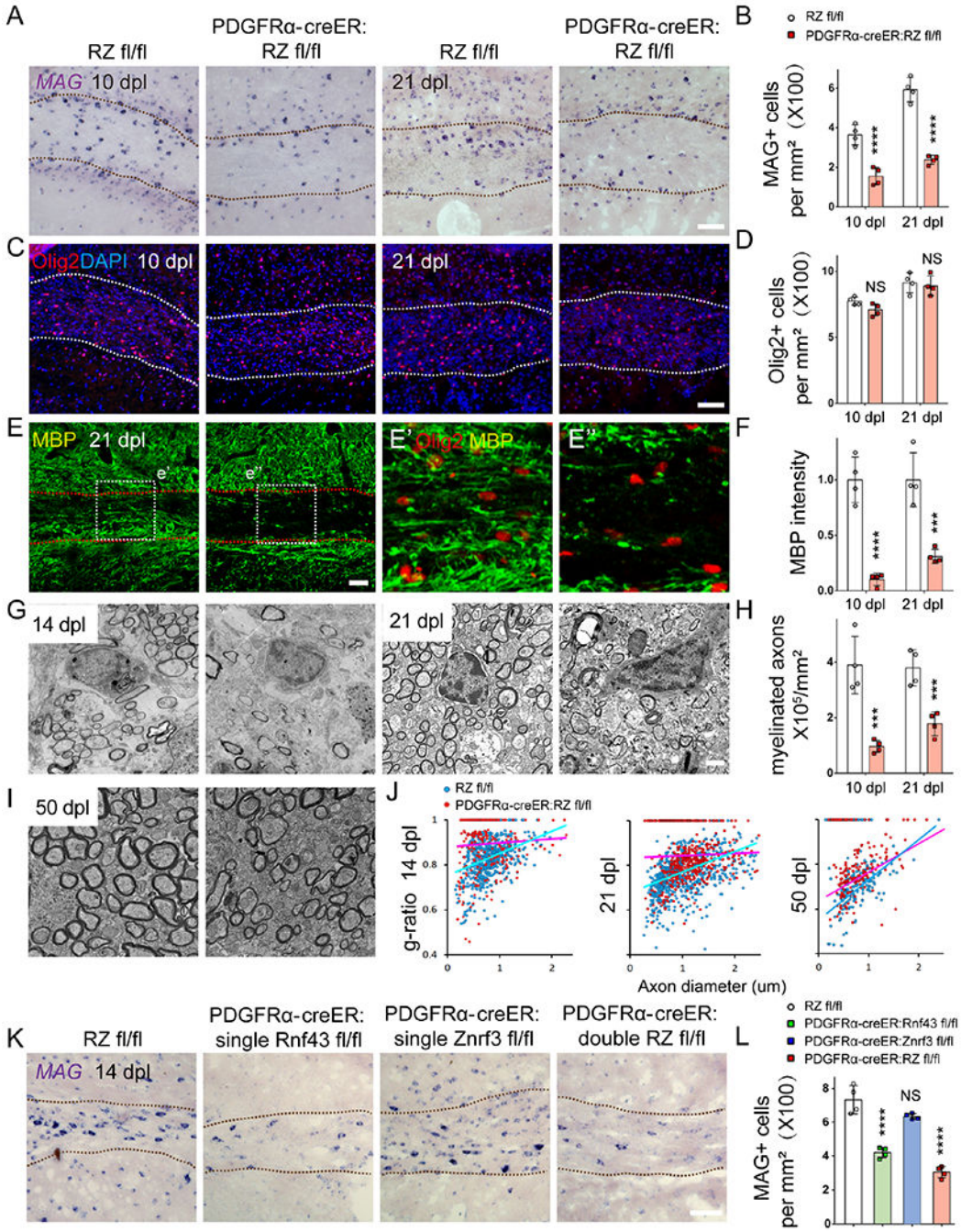

Fig. 4: Rnf43 function is critical for remyelination

(A, B) *MAG+* mRNA expressing OLs at 10 days post lesioning (dpl) and 21 dpl following lysolecithin induced corpus callosum focal demyelination in induceable PDGFRα-creER:RZfl/fl mice and RZfl/fl control (non cre) mice (lesioning schematic Fig. S4A), and (B) quantification of *MAG+* cells in lesion areas. Dotted line marks lesion extent in corpus callosum. (C) DAPI staining and Olig2 immunohistochemistry identifies lesion area and oligodendroglial cell numbers in lesions respectively in the same mice as above, and (D) quantification of Olig2+ cells in lesion areas at 10dpl and 21dpl. (E) MBP

Immunostaining in lesions at 21dpl in PDGFRα-creER:RZfl/fl and RZfl/fl control mice (enlargements shown in E' and E") with (F) quantification of MBP intensities at 10dpl and 21dpl in lesions. (G) Electron microscopy (EM) of remyelination at 14 dpl and 21 dpl in PDGFRα-creER:RZfl/fl and RZfl/fl/control mice, with (H) quantification of myelinated axons in lesions from these same mice (n=4 animals). (I) EM of remyelination at 50 dpl in PDGFRα-creER:RZfl/fl and RZfl/fl control mice. (J) G-ratio analyses of remyelination at 14dpl, 21dpl and 50dpl (scatterplot displays g-ratios of individual axons as a function of axonal diameter. n=4 animals) in PDGFRα-creER:RZfl/fl and RZfl/fl/ control lesions (solid lines show linear trend lines). (K) *MAG+* mRNA expressing OLs at 14 dpl following lysolecithin induced corpus callosum focal demyelination in PDGFRα-creER:RZfl/fl double mutant mice, PDGFRα-creER:Rnf43 fl/fl single mutant mice, PDGFRα-creER:Znrf3 fl/fl single mutant mice, and RZfl/fl control mice (non cre), and (L) quantification of *MAG+* cells in lesion areas. Values in all graphs are mean±s.d. NS not significant, *$p<0.05$, ** $p<0.01$, *** $p<0.001$, **** $p<0.0001$. Scale bars in all images are 100μm, except in (G) which is 100μm. See also Fig. S4, S5 and S6.

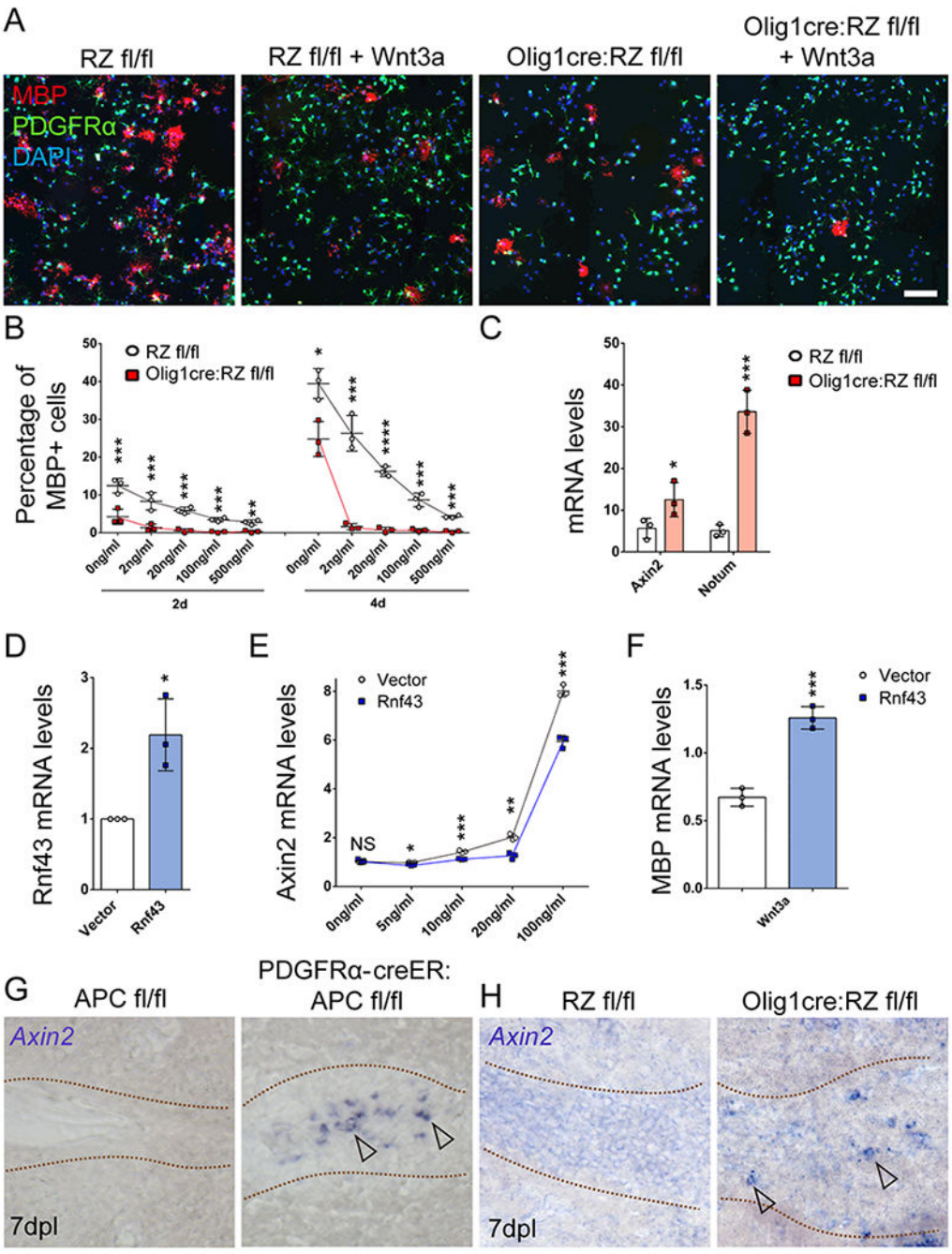

Fig. 5: Rnf43 controls OPC differentiation through negative regulation of Wnt

(A) Differentiation of Pdgfrα (green) OPCs into mature MBP (red) expressing OL, from OPCs isolated from RZ fl/fl control and Olig1cre:RZ fl/fl mice, in the presence (+Wnt3a) or absence of Wnt3a added to the media. (B) Quantification of OPC differentiation into MBP+ cells from the above RZ fl/fl control and Olig1cre:RZ fl/fl mice when treated with increasing concentrations (marked on x axis) of Wnt3a (n=3 independent experiments). Numbers are expressed as percentage of total cells that were MPB+. (C) qPCR for Wnt targets *Axin2* and *Notum* mRNA in RZ fl/fl OPCs and Olig1cre:RZ fl/fl OPCs with 100ng/ml Wnt3a

treatment, depicted as fold change normalized to the mRNA levels in RZ fl/fl OPCs without Wnt3a treatment (n=3 independent experiments). (D) qPCR for *Rnf43* mRNA expression levels in the Oli-neu oligodendroglial cell line transfected with control vector or Rnf43 expression vector (n=3 independent experiments). (E) Wnt target *Axin2* mRNA levels in Oli-neu cells transfected with control vector or Rnf43 expression vector in the presence of increasing Wnt3a stimulation (concentrations marked on x axis; n=3 independent experiments). (F) *MBP* mRNA levels in Oli-neu cells treated with Wnt3a and transfected with either control vector or Rnf43 expression vector (n = 3 independent experiments). (G) *Axin2* mRNA is significantly upregulated (arrowheads) in 7dpl remyelinating lesions (lesion boundaries marked with dotted lines) from both PDGFRα-creER:APCfl/fl (G) and Olig1cre:RZfl/fl (H) mice compared to their respective APCfl/fl and RZfl/fl non cre controls. Values in all graphs are mean±s.d. NS not significant, *p<0.05, ** p<0.01, *** p<0.001. Scale bar in (A) is 100μm. See also Fig. S7.

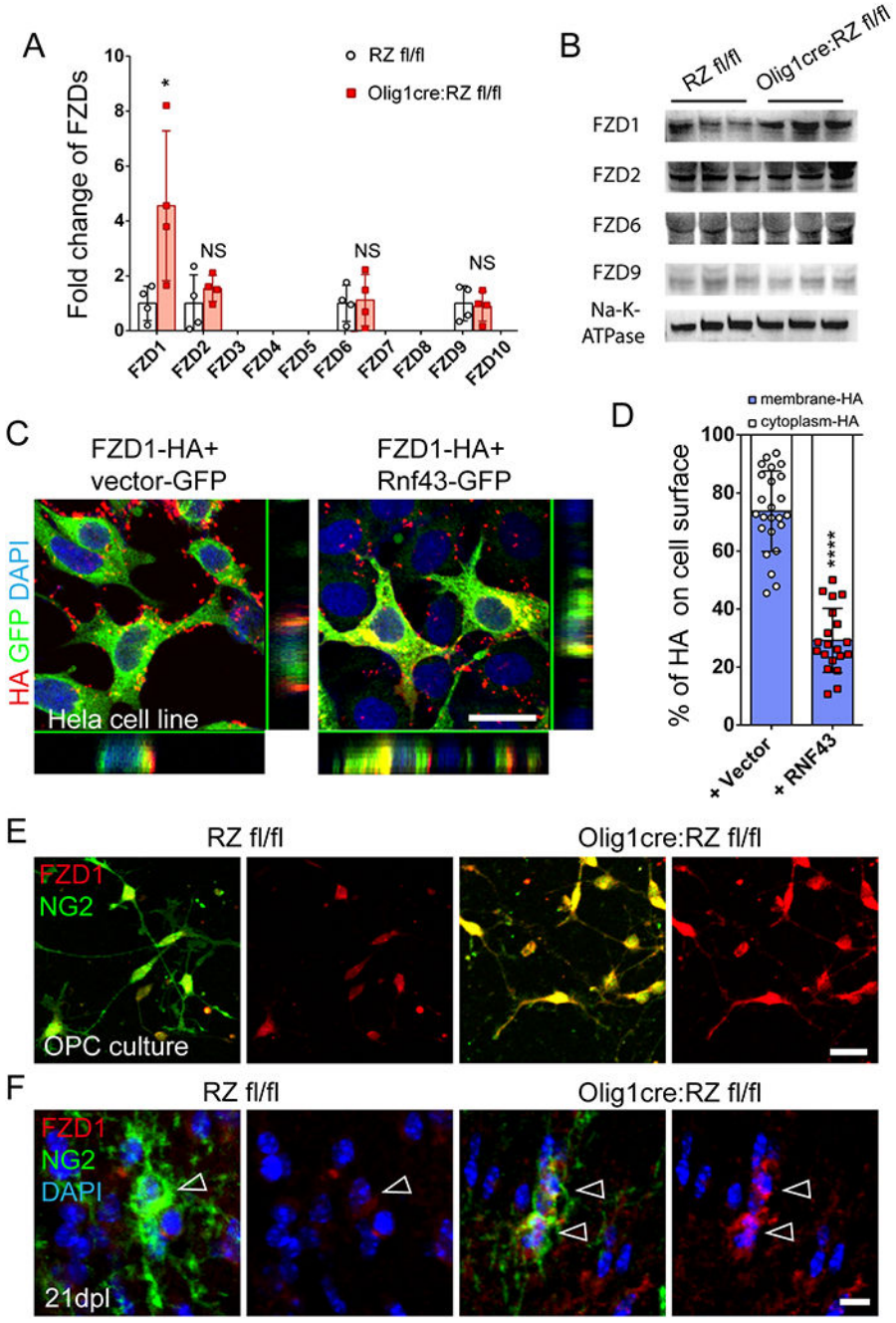

Fig. 6: Rnf43 regulates OPC Fzd1 surface expression

(A) Quantification of western blots for Fzd1-10 protein levels in surface membrane extractions from Olig1cre:RZ fl/fl and RZ fl/fl control OPCs (n=4 independent experiments). Na-K-ATPase was used as loading control. (B) Western blot for Fzd1, Fzd2, Fzd6 and Fzd9 (n=4 independent experiments) in Olig1cre:RZ fl/fl and RZ fl/fl control OPC membranes. (C) Immunostaining for HA and GFP tags (and DAPI) in hela cells transfected with the following vectors: left, FZD1-HA and empty control vector-GFP; right, FZD1-HA and Rnf43-GFP. The location of FZD1 is indicated by HA tag localization.

(D) Quantification from the above vector transfections in (C) of Fzd1 localization on cell membrane or in cytoplasm by quantification of HA+ foci (n=3 independent experiments). (E) FZD1 (red) expression in NG2+ OPCs (green) in vitro following isolation from Olig1cre:RZ fl/fl and RZ fl/fl control mice (E), and in vivo in 21dpl remyelinating corpus callosum lesions from these same mice. Values in graphs are mean±s.d. NS not significant, *p<0.05, **** p<0.0001. Scale bars are 20μm (in c, e) and 10μm in (f). See also Fig. S7.

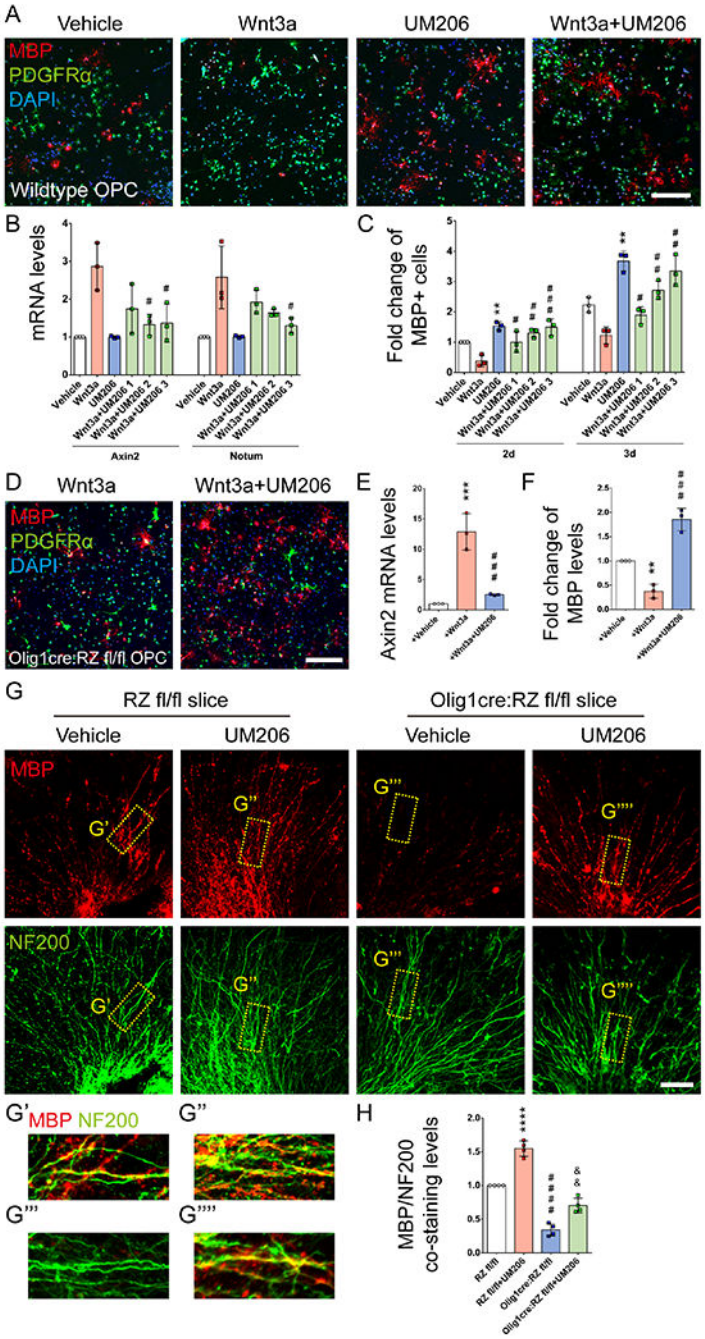

Fig. 7: Fzd1 inhibition via UM206 promotes OPC differentiation and ex vivo remyelination

(A) Differentiation of wildtype PDGFRα (green)+ OPCs into mature MBP (red)+ OLs with treatments of vehicle control, 100ng/ml Wnt3a, 100nM UM206, or combination Wnt3a/UM206. Scale bar 200μm. (B) qPCR for Wnt targets *Axin2* and *Notum* mRNA in wildtype OPCs with treatments of vehicle control, Wnt3a alone, UM206 alone, and 100ng/ml Wnt3a with serial concentrations of UM206 (UM206 1: 1nM; UM206 2: 10nM; UM206 3: 100nM). #: compared to Wnt3a; n=3 independent experiments. (C) Quantification of OPC differentiation into MBP+ OLs under the same treatment conditions as described in

(B). * : compared to Vehicle; #: compared to Wnt3a; n=3 independent experiments. (D) Differentiation of PDGFRα (green)+ OPCs (isolated from Olig1cre:RZ fl/fl mice) into mature MBP (red)+ OLs with treatments of 100ng/ml Wnt3a alone or in combination with 100nM UM206. Scale bar 200μm. (E) qPCR for Wnt target *Axin2* mRNA in vehicle treated Olig1cre:RZ fl/fl OPCs, or Olig1cre:RZ fl/fl OPCs under the two different treatments conditions shown in (D). * : compared to Vehicle; #: compared to Wnt3a; n=3 independent experiments. (F) Quantification of Olig1cre:RZ fl/fl OPC differentiation into MBP+ OLs under the same treatment conditions as in (E). *: compared to Vehicle; #: compared to Wnt3a; n=3 independent experiments. (G) Remyelination of MBP (red)+ myelin sheaths on NF200 (green)+ nerve fibers at 10 days after a lysolecithin-induced demyelination of cerebellar slice culture from RZ fl/fl control and Olig1cre:RZ fl/fl mice, with either vehicle treatment or 100nM UM206 (slice culture treatment schematic Fig. S4B). Scale bar 100μm. G' to G"" shows magnifications of the overlaid MBP/NF200 staining from the boxed areas marked in (G). (H) Quantification of MBP/NF200 co-staining as an indication of the myelin regeneration under the four conditions shown in (G). ****: RZ fl/fl+UM206 vs. RZ fl/fl; ####: Olig1cre:RZ fl/fl vs. RZ fl/fl; &&: Olig1cre:RZ fl/fl+UM206 vs.Olig1cre:RZ fl/fl. n=4 independent experiments. Values are mean±s.d. NS not significant, *p<0.05, ** p<0.01, *** p<0.001, **** p<0.0001. See also Fig. S4 and S8.

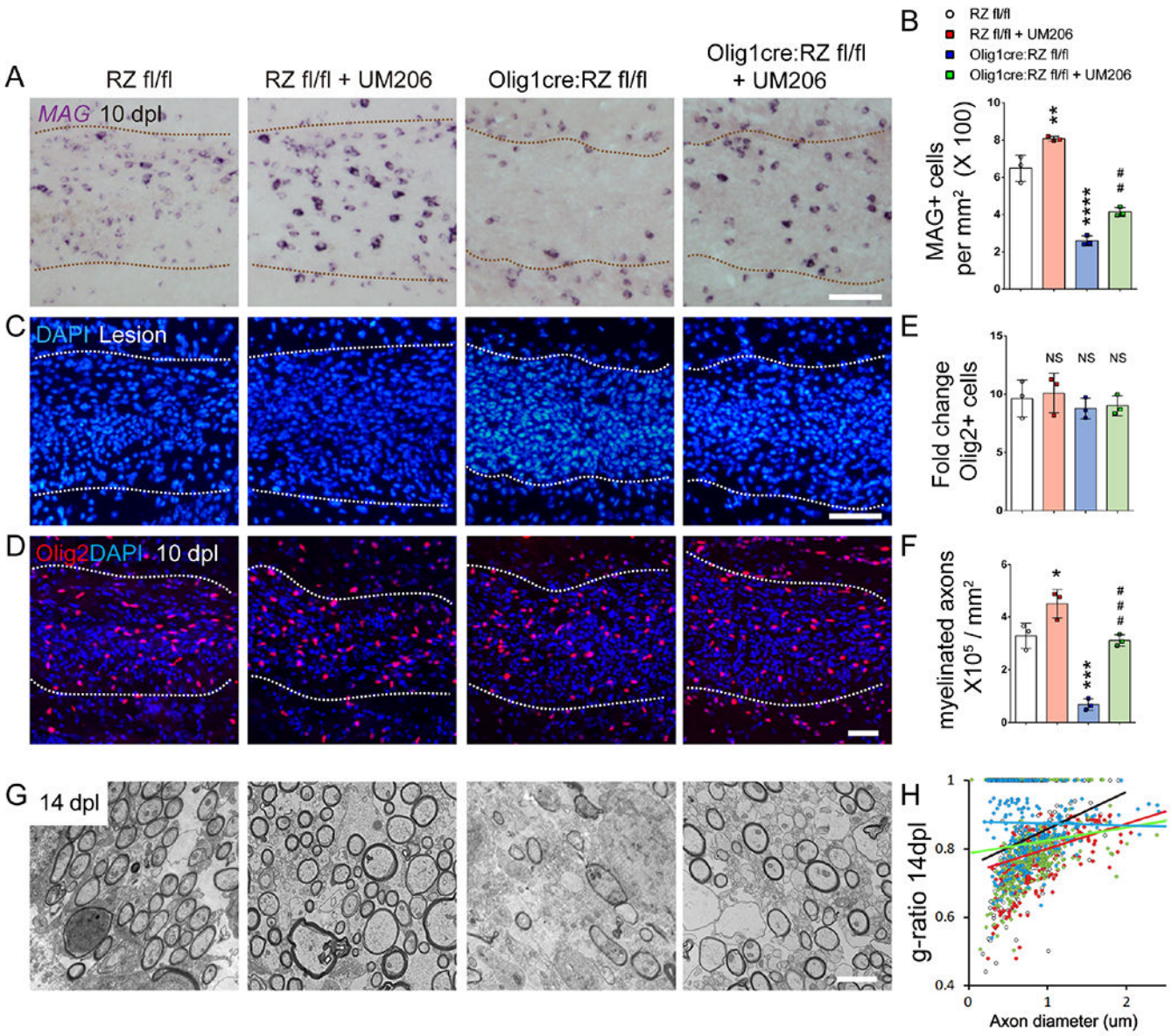

Fig. 8: Fzd1 inhibition via UM206 promotes in vivo remyelination

(A, B) *MAG+* mRNA expressing cells at 10 dpl following lysolecithin induced corpus callosum focal demyelination with or without UM206 infusion in either Olig1cre: RZfl/fl mice or control RZfl/fl (non cre)(lesioning schematic Fig. S4C, S4D), and (B) quantification of *MAG+* cells in lesion areas. Dotted line marks lesion extent in corpus callosum. * : compared to RZ fl/fl; #: compared to Olig1cre:RZ fl/fl. (C) DAPI staining identifies lesion areas in the same mice as above. (D) Olig2+ immunostaining in lesion areas from above mice, with quantification in (E). (F) Quantification (from EM) of myelinated axons in lesions at 14 dpl. * : compared to RZ fl/fl; #: compared to Olig1cre:RZ fl/fl. (G) EM of remyelination at 14 dpl from these same mice. (H) G-ratio analyses of remyelination at 14dpl (scatterplot displays g-ratios of individual axons. n=3 animals). Values in all graphs

are mean±s.d. NS not significant, *p<0.05, ** p<0.01, *** p< 0.001, **** p<0.0001. Scale bars in all images are 100μm, except in (G) which is 1μm. See also Fig. S4 and S8.

KEY RESOURCES TABLE

REAGENT or RESOURCE	SOURCE	IDENTIFIER
Antibodies		
Rat anti-PDGFRα	BD Biosciences	Cat# 558774, RRID:AB_397117
Rabbit anti-PDGFRα	Gift from W. Stallcup	Kucharova et al., 2011
Rabbit anti-Olig2	Gift from C.D. Stiles	Arnett et al., 2014
Rabbit anti-RNF43	Abcam	Cat# ab84125, RRID:AB_2181252
Rabbit anti-NF200	Sigma-Aldrich	Cat# N4142, RRID:AB_477272
Rabbit anti-Rnf43	Abcam	Cat# ab217787
Rat anti-FZD1	R&D	Cat# MAB11201
Rat anti-MBP	Serotec	Cat# MCA409S
Mouse anti-NG2	Millipore	Cat# 05-710, RRID:AB_11214068
Rabbit anti-Ki67	Thermo Fisher scientific	Cat# MA5-14520, RRID:AB_10979488
Mouse anti-Olig2	Millipore	Cat# MABN50, RRID:AB_10807410
Mouse anti-HA	Beyotime	Cat# AH158
Goat anti-FZD2	Invitrogen	Cat# PA5-47119
Goat anti-FZD3	R&D	Cat# AF1001
Rat anti-FZD4	R&D	Cat# MAB194
Rabbit anti-FZD5	Abcam	Cat# ab75234, RRID:AB_1523637
Mouse anti-FZD6	Santa Cruz	Cat# sc-393791, RRID:AB_2736833
Rabbit anti-FZD7	Novus Biologicals	Cat# NBP2-23624
Rabbit anti-FZD8	Novus Biologicals	Cat# NLS4767, RRID:AB_2109536
Goat anti-FZD9	R&D	Cat# AF2440
Rabbit anti-FZD10	Abcam	Cat# ab83044, RRID:AB_1860570
Rabbit anti-Na-K-ATPase	Cell signaling technology	Cat# 3010, RRID:AB_2060983
Rabbit Anti-Rnf43	Invitrogen	Cat# PA5-79930
Normal Rabbit IgG	Cell signaling technology	Cat# 2729S
Sheep anti-Digoxigenin-AP Fab fragments	Sigma-Aldrich	Cat# 11093274910
Biological samples		
Human MS Tissue	Imperial College London, MS Brain Bank, UK	http://www.imperial.ac.uk/medicine/multiple-sclerosis-and-parkinsons-tissue-bank
Human newborn HIE tissue and controls	UCSF Pediatric Neuropathology Research Laboratory (PNRL)	https://pediatrics.ucsf.edu/neonatology/newborn-brain-research-institute
Chemicals, peptides, and recombinant proteins		
Tamoxifen	Sigma-Aldrich	Cat# T5648
Lysolecithin	Sigma-Aldrich	Cat# L4129
UM206	ChinaPeptides	Laeremans et al., 2011
Recombinant Murine Wnt3a	PeproTech	Cat# 315-20,
Human recombinant PDGF-AA	PeproTech	Cat# 100-13A

REAGENT or RESOURCE	SOURCE	IDENTIFIER
Critical commercial assays		
NBT/BCIP Stock Solution	Sigma-Aldrich	Cat# 11681451001
Amaxa Nucleofector Kit	Lonza	Cat# VPI-1006
Mem-PER™ Plus Membrane Protein Extraction Kit	Thermo Fisher scientific	Cat# 89842
ECL™ Prime Western blotting detection reagents	GE Healthcare	Cat# RPN2232
RNeasy Plus Mini Kit	Qiagen	Cat# 74134
GoTaq® qPCR Master Mix	Promega	Cat# A6001
Protein A/G PLUS-Agarose	Santa Cruz	Cat# sc-2003, RRID:AB_10201400
Experimental models: Cell lines		
Hela cell line	ATCC	CCL-2
Oli-neu cell line	Jung et al., 1995	N/A
Experimental models: Organisms/strains		
Mouse: Rnf43 fl/fl	Koo et al., 2012	N/A
Mouse: Znrf3 fl/fl	Koo et al., 2012	N/A
Mouse: Olig1-cre	Arnett et al., 2004	N/A
Mouse: Olig2-cre	Schuller et al., 2008	N/A
Mouse: PDGFRa-creER	Kang et al., 2010	N/A
Mouse: Rosa-YFP	Jackson laboratory	Cat# 006148
Mouse: Aldh1L1-GFP	Jackson laboratory	Cat# 030248
Mouse: Cx3cr1-GFP	Jackson laboratory	Cat# 032127
Mouse: APC fl/fl	Robanus-Maandag et al., 2010	Cat# 029275
Oligonucleotides		
Primer: Rnf43 Forward: CAGCCAGTGTGGTTGTATCT Reverse: ACCTGGCAATGTGAGTAAGG	This paper	N/A
Primer: Znrf3 Forward: TCTCTTCTGTGCCCTCTTCT Reverse: GCTCCTTGTCCATGGCTATAC	This paper	N/A
Primer: Axin2 Forward: CCAGGTGGACCAAGTCTTTAC Reverse: TCATCTGCCTGAACCCATTAC	This paper	N/A
Primer: Notum Forward: AACGTGGCACAGTTCCTTAT Reverse: CACACCCTCTAGTTCCCATTAC	This paper	N/A
Primer: Olig2 Forward: GGCGGTGGCTTCAAGTCATC Reverse: TCGGGCTCAGTCATCTGCTTC	This paper	N/A
Primer: PDGFRα Forward: GGGGAGAGTGAAGTGAGCTG Reverse: CATCCGTCTGAGTGTGGTTG	This paper	N/A
Primer: MBP Forward: AATGCGGAAAGGAAGGAGAG Reverse: TGTCCGATCAGGGCTAGTAT	This paper	N/A
Primer: GAPDH Forward: AGGCCGGTGCTGAGTATGTC Reverse: TGCCTGCTTCACCACCTTCT	This paper	N/A
Recombinant DNA		
Plasmid: FZD1-HA	This paper	N/A
Plasmid: Rnf43-GFP	This paper	N/A
Software and algorithms		

REAGENT or RESOURCE	SOURCE	IDENTIFIER
Image-Pro Plus software 5.0	Media Cybernetics	https://www.mediacy.com/imageproplus; RRID: SCR_007369
GraphPad Prism 6	GraphPad Software	https://www.graphpad.com/scientificsoftware/prism/; RRID:SCR_015807
ZEN Digital Imaging for Light Microscopy	Zeiss	RRID:SCR_013672
Olympus Confocal Laser Scanning Microscope software	Olympus	RRID:SCR_017015